Probing transverse-momentum distributions with groomed jets

Daniel Gutierrez-Reyes,[a] Yiannis Makris,[b] Varun Vaidya,[b] Ignazio Scimemi[a] and Lorenzo Zoppi[c,d]

[a] *Departamento de Física Teórica and IPARCOS, Universidad Complutense de Madrid (UCM),*
 E-28040 Madrid, Spain

[b] *Theoretical Division, MS B283, Los Alamos National Laboratory,*
 Los Alamos, NM 87545, U.S.A.

[c] *Institute for Theoretical Physics Amsterdam and*
 Delta Institute for Theoretical Physics University of Amsterdam,
 Science Park 904, 1098 XH Amsterdam, The Netherlands

[d] *Nikhef, Theory Group,*
 Science Park 105, 1098 XG, Amsterdam, The Netherlands

 E-mail: dangut01@ucm.es, yiannis@lanl.gov, vvaidya@lanl.gov,
 ignazios@fis.ucm.es, L.Zoppi@uva.nl

ABSTRACT: We present the transverse momentum spectrum of groomed jets in di-jet events for e^+e^- collisions and semi-inclusive deep inelastic scattering (SIDIS). The jets are groomed using a soft-drop grooming algorithm which helps in mitigating effects of non-global logarithms and underlying event. At the same time, by reducing the final state hadronization effects, it provides a clean access to the non-perturbative part of the evolution of transverse momentum dependent (TMD) distributions. In SIDIS experiments we look at the transverse momentum of the groomed jet measured w.r.t. the incoming hadron in the Breit frame. Because the final state hadronization effects are significantly reduced, the SIDIS case allows to probe the TMD parton distribution functions. We discuss the sources of non-perturbative effects in the low transverse momentum region including novel (but small) effects that arise due to grooming. We derive a factorization theorem within SCET and resum any large logarithm in the measured transverse momentum up to NNLL accuracy using the ζ-prescription as implemented in the `artemide` package and provide a comparison with simulations.

Contents

1 Introduction

The understanding of the structure of nucleons is one of the most important and interesting research subject in modern nuclear physics. The ultimate goal would be to have a complete description of quarks/gluons position and momenta inside a hadron, which is not easy because of the entanglement of initial/final states in all hadronic processes. In order to properly define all hadron constituent contributions, the cross sections should be factorized in some region of the phase space into properly defined hadronic matrix elements. Here we will consider the transverse momentum dependent distributions (TMD), which appear in the factorization of several processes like Drell-Yan, semi-inclusive deep-inelastic-scattering (SIDIS) and e^+e^- hadron production [1–5]. Drell-Yan processes directly test the TMD parton distribution functions (TMDPDF), while in SIDIS cross sections the TMDPDFs are coupled to a TMD fragmentation function in the final state. Finally in e^+e^- hadron production only the TMD fragmentation is present. Because of the factorization theorem, the TMDs have several universal features like rapidity and renormalization scale evolution, which should be also tested including their (universal) non-perturbative part. Recently some of us have considered the possibility to define a jet-TMD, replacing a final state hadron with a jet [6–8] in SIDIS and e^+e^- processes. The check of this possibility has revealed that standard jet definitions are compatible with a factorization theorem only in the case of small enough radii, which is a not obvious experimental condition in the planned electron-hadron collider like EIC or LHeC. Instead large jet-radii need a specific definition of jet, which allows soft radiation to be independent of radius. In [7, 8] this was achieved using the winner-take-all (WTA) axis [9], and the perturbative calculations were done with a precision similar to the case of fragmenting hadrons.

In this work we consider the possibility of groomed jets in SIDIS or $e^+e^- \to 2$ jets. Developments in jet substructure have shown that applying a grooming algorithm to a jet, using for example the so called "soft-drop" procedure, robustly removes the contamination from both underlying event and non-global correlations. Since this process essentially removes wide angle soft radiation, retaining only a collinear core, it also dramatically reduces hadronization effects (see figure 1), thus allowing an easier access to the TMD non-perturbative physics which we want to probe. Groomed jets with an identified light/heavy hadron in the jet were also proposed as probes of TMD evolution and distribution in [10, 11]. The residual non-perturbative effects contain pieces that depend on the soft-drop grooming procedure and require careful analysis as was pointed out in [12]. In addition, with the use of soft-drop we can derive factorization theorems for large jet radius ($R \sim 1$), which we consider to be the relevant case for low energy experiments, such as EIC. In order to focus on collimated jet configurations, we also impose an upper cutoff in the groomed jet invariant mass.[1] This constraint allows us to derive a factorization theorem involving the same universal soft function that appears in traditional hadronic TMD, and which is independent of the jet radius for $R \sim 1$. This is a key feature for groomed jets and it is necessary for the universality of TMDs and for this reason, in this paper, we only consider

---

[1]Note that the small transverse momentum constraint does not necessarily ensure collimated configurations since topologies with two or more widely separated sub-jets are also permitted.
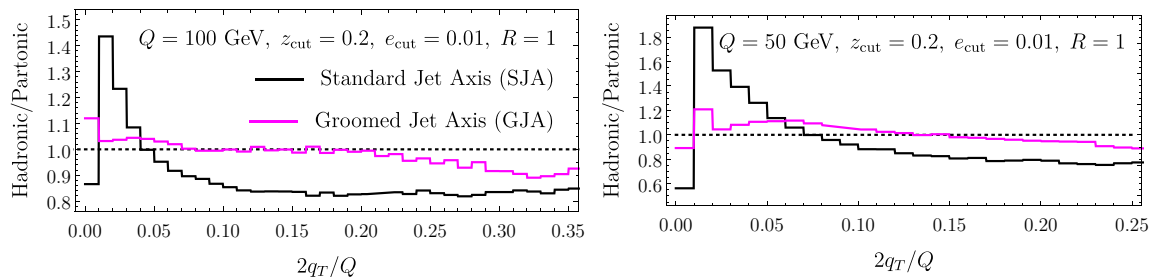
Figure 1. Hadronization effects in a typical $e^+e^- \to 2$ jets from PYTHIA 8 [13, 14]. at center of mass values, LEFT: $Q = 100\,\text{GeV}$, RIGHT: $Q = 50\,\text{GeV}$.

$R \sim 1$. The cutoff is imposed using groomed jet-thrust, $e \equiv (m/Q)^2$, where m is the groomed invariant mass and Q is the center of mass energy. This allows us to introduce a single cutoff parameter, e_{cut}, independent of the jet energy or transverse momentum.

The paper is organized as follows. In section 2, we give a review of soft-drop and discuss the factorization of the $e^+e^- \to 2$ jets, transverse momentum decorrelation within SCET and give detailed comparisons of our NNLL accurate prediction with simulations for this observable. In section 3, we consider the factorization for the corresponding observable in DIS. We carefully enumerate all the non-perturbative corrections and discuss their universality in section 4. We conclude in section 5. The details of the one loop calculations, resummation, and evolution are provided in the appendix.

2 Di-jet events in electron-positron colliders

In this section we discuss the measurement of momentum de-correlation in electron-positron colliders. We identify events with two final state jets and we consider the transverse momentum of one jet w.r.t. the other. The measurement that we are considering in this work is a generalization of the di-hadron momentum de-correlation,

$$\boldsymbol{q}_T = \frac{\boldsymbol{p}_{Th_1}}{z_1} + \frac{\boldsymbol{p}_{Th_2}}{z_2} \tag{2.1}$$

where one or both of the identified hadrons is replaced by a jet, defined through an infrared-safe jet algorithm. Here $\boldsymbol{p}_{Th_i}$ and z_i are the transverse momentum and energy fraction of the hadron i respectively. The factorization theorem is usually written for this normalized vector sum of the transverse momenta rather than just the sum of the transverse momenta. It can be verified by momentum conservation and simple geometry that the quantity $\boldsymbol{p}_{Th_1}/z_1$ represents the transverse momentum of the radiation recoiling against the hadron w.r.t. the axis defined by the hadron itself. This makes it convenient to write a factorization theorem which matches onto the standard hadron fragmentation function as explained in [10].

We consider three possible scenarios as illustrated in figure 2 and we refer to them as di-hadron, hadron-jet, and di-jet momentum de-correlation. To simplify the discussion we focus on the case of di-jets (figure 2c) and we briefly comment how our results are generalized for the case of hadron-jet de-correlation. For the case of groomed jets the
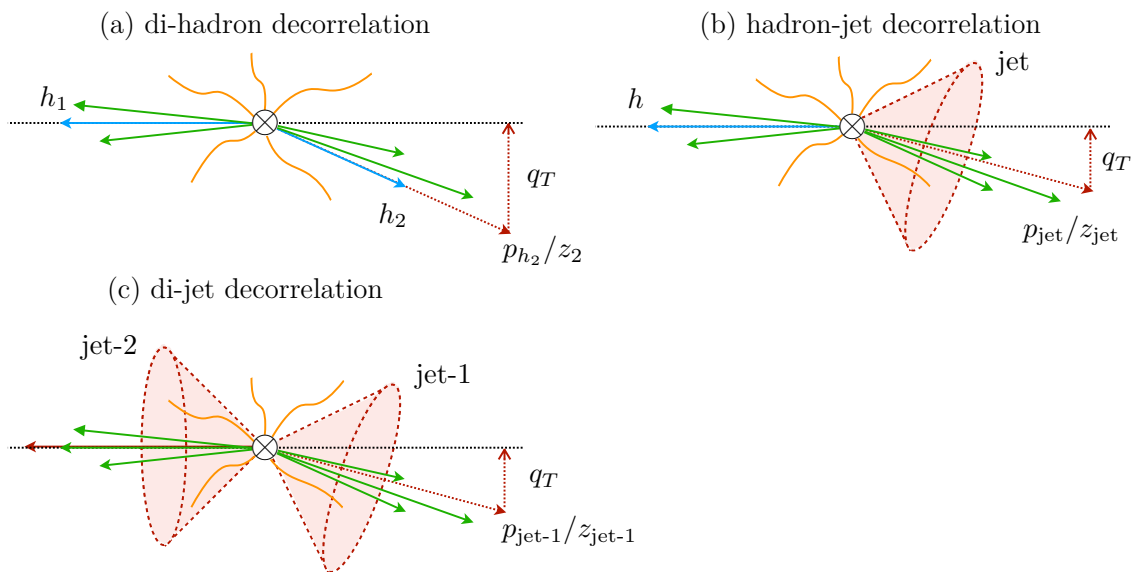
Figure 2. Three possible transverse momentum de-correlation measurements in e^+e^- annihilation: (a) Identify two hadrons h_1 and h_2 with momenta p_{h_1}, p_{h_2} and energy fractions z_{h_1}, z_{h_2} respectively, (b) Identify a jet and a hadron with momenta p_{jet}, p_h with energy fractions z_{jet}, z_h, (c) Identify two jets with momenta $p_{\text{jet}_1}, p_{\text{jet}_2}$ and energy fractions $z_{\text{jet}_1}, z_{\text{jet}_2}$.

observable $\boldsymbol{q}_T$ is defined with the groomed quantities, i.e., p_{jet}^μ is the *groomed* jet four-momentum and $z_{\text{jet}} = 2p_{\text{jet}}^0/Q$. The transverse component $\boldsymbol{p}_{T\,\text{jet}}$ is measured with respect to an axis close to the full or groomed jet axes. The exact choice of the axis only differs by power corrections. For concreteness in the results that follow we make the choice of the axis to lie along one of the groomed jets.

Since we want to probe the non-perturbative physics, we wish to work in the small transverse momentum regime ($q_T \ll \sqrt{s}$ where $q_T \equiv |\boldsymbol{q}_T|$). There are various ways one can define the jet axis and the choice of definition will impact the form of factorization. It was discussed in ref. [7] that the standard jet axis choice suffers from factorization breakdown for large jet radius. This breakdown is due to energetic emissions at relatively wide angles. Such configurations will contribute to the small transverse momentum region when the energetic subjets are clustered in a single large radius jet. To avoid this problem in refs. [7, 8] the winner-take-all (WTA) axis was used instead. This way ensures that wide angle energetic emissions induce large transverse momentum ($q_T \sim \sqrt{s}$) pushing the q_T measurement away from the observable region.

In this paper we propose, alternatively, the use of groomed jet-substructure to isolate the collimated configurations and choose the jet axis to be the groomed jet axis which is insensitive to jet boundary effects. Particularly we consider the normalized jet mass as the relevant jet-substructure observable,

$$e \equiv \left(\frac{m_J}{Q}\right)^2 . \tag{2.2}$$

We shall see that imposing this constraint still allows us to capture a majority of events and hence does not significantly impact the cross-section.

2.1 Soft-drop: a brief review

The grooming procedure that we use is the soft-drop algorithm. We give here a brief review of the soft-drop groomer and eventually discuss the various hierarchies, the relevant modes and the factorization of the cross section in the next sections.

Soft-drop grooming [15] removes contaminating soft radiation from the jet by constructing an angular ordered tree of the jet, and removing the branches at the widest angles which fail an energy requirement. The angular ordering of the jet is constructed through the Cambridge/Aachen (C/A) clustering algorithm [16–20]. As soon as a branch is found that passes the test, it is declared the groomed jet, and all the constituents of the branch are the groomed constituents. At the end of the grooming procedure only the narrow energetic core remains from the original jet. Since at large angles all collinear energetic radiation is to be found at the center of the jet, no cone is actually imposed to enclose this core. One simply finds the branch whose daughters are sufficiently energetic. Formally the daughters could have any opening angle, though their most likely configuration is collinear.

The strict definition of the algorithm is as follows. Given an ungroomed jet (which itself is identified first using a suitable algorithm such as the anti-k_T, [21]), first we build the clustering history by starting with a list of particles in the jet. At each stage we merge the two particles within the list that are closest in angle.[2] This gives a pseudo-particle, and we remove the two daughters from the current list of particles, replacing them with the merged pseudo-particle. This is repeated until all particles are merged into a single parent. Then we open the tree back up working backwards so that at each stage of the declustering, we have two branches available, label them i and j. We require:

$$\frac{\min\{E_i, E_j\}}{E_i + E_j} > z_{\text{cut}} \left(\frac{\theta_{ij}}{R}\right)^\beta, \tag{2.3}$$

where z_{cut} is the modified mass drop parameter, β is the parameter which controls the angularities, θ_{ij} is the angle between i^{th} and j^{th} particle, R is the jet radius and E_i is the energy of the branch i. If the two branches fail this requirement, the softer branch is removed from the jet, and we decluster the harder branch, once again testing eq. (2.3) within the hard branch. The pruning continues until we have a branch that when declustered passes the condition eq. (2.3). All particles contained within this branch whose daughters are sufficiently energetic constitute the groomed jet. Intuitively we have identified the first genuine collinear splitting.

For a hadron-hadron collision, one uses the transverse momentum (p_T) with respect to the beam for the condition of eq. (2.3),

$$\frac{\min\{p_{Ti}, p_{Tj}\}}{p_{Ti} + p_{Tj}} > z_{\text{cut}} \left(\frac{\theta_{ij}}{R}\right)^\beta. \tag{2.4}$$

We formally adopt the power counting $z_{\text{cut}} \ll 1$, though typically one chooses $z_{\text{cut}} \sim 0.1$. See [24] for a study on the magnitude of the power corrections with respect

---

[2]This merging is usually taken to be summing the momenta of the particles, though one could use winner-take-all schemes [9, 22, 23].

to z_{cut} for jet mass distributions. To be specific, in this paper we consider only the case $\beta = 0$. Note that for $\beta = 0$ the energy of the groomed jet constituents is a collinear unsafe observable [15, 25], however, the additional constraint of the measured transverse momentum $\boldsymbol{q}_T$ provides a physical collinear cutoff in a similar way a jet shape measurement does. For detailed discussion on this we refer to appendix D.

2.2 Hierarchies, modes, and factorization

In order to compute the transverse momentum de-correlation $\boldsymbol{q}_T$, defined in eq. (2.1), for two groomed jets in di-jet events in e^+e^- annihilation (figure 2 (c)) we are going to impose a normalized jet mass measurement as defined in eq. (2.2) on both jets. The other parameters that enter our cross section are the soft-drop parameters $z_{\text{cut}} \sim 0.1$, $\beta = 0$. Ultimately we are going to integrate over the jet mass measurement up to an appropriate (but still small) cut-off value e_{cut}.

We have a rich spectrum of possible hierarchies of momenta, which are all consistent with maintaining $q_T/Q, e_{\text{cut}}, z_{\text{cut}} \ll 1$. We have that $q_T/Q, e_{\text{cut}}, z_{\text{cut}}$ are now expansion parameters in the effective field theory (EFT), and they should be taken into account in the factorization of the process. We first list and briefly discuss these hierarchies and the corresponding factorization theorems within an EFT. The general modes that we will consider will fall into three classes. Modes that explicitly pass soft drop (usually the highly energetic collinear modes), modes that explicitly fail soft-drop (the global soft function modes) and finally those which can live on the border and need to be tested, as to whether they pass or fail. Only the modes that pass soft-drop will contribute to e, while $\boldsymbol{q}_T$ receives contributions from all radiation that fails soft-drop.

The first regime in which we are interested is $Q \gg Q z_{\text{cut}} \gg q_T \gtrsim Q\sqrt{e} \gg Q\sqrt{e z_{\text{cut}}}$. Here we have low values of q_T which are of the order of $Q\sqrt{e}$. We identify the following modes to be relevant to the cross section:

$$\text{soft:} \quad p_s^\mu \sim q_T(1,1,1);$$
$$\text{collinear:} \quad p_c^\mu \sim Q(\lambda_c^2, 1, \lambda_c), \ \lambda_c = \sqrt{e}, \tag{2.5}$$

and the factorization of the cross section in this region is schematically

$$\frac{d\sigma}{de_1 de_2 d\boldsymbol{q}_T} = H_2^{ij}(Q;\mu) \times S(\boldsymbol{q}_T) \otimes \mathcal{J}_i^\perp(e_1, Q, z_{\text{cut}}, \boldsymbol{q}_T) \otimes \mathcal{J}_j^\perp(e_2, Q, z_{\text{cut}}, \boldsymbol{q}_T). \tag{2.6}$$

Apart from the hard factor H all the other terms in this equation are affected by rapidity divergences. The global soft function S that appears in the factorization theorem in eq. (2.6) (and later in the SIDIS case eq. (3.4)) is the universal function that is also present in the factorization theorem of Drell-Yan, di-hadron production in electron-positron annihilation, and semi-inclusive DIS with TMDs. The operator definition of the soft function (see refs. [1, 2, 26]) is given by

$$S(\boldsymbol{q}_T) = \frac{1}{N_R} \text{tr} \langle [S_n^\dagger S_{\bar{n}}](0) \delta^{(2)}(\boldsymbol{q}_T - \boldsymbol{\mathcal{P}}_\perp)[S_{\bar{n}}^\dagger S_n](0) \rangle, \tag{2.7}$$

where $N_R = N_c$ for $S_{n/\bar{n}}$ in the fundamental and $N_c^2 - 1$ for the adjoint representation of $\text{SU}(N_c)$. This function has been calculated at NNLO in [27]. This function is responsible

for the TMD evolution which is actually known up to third order [28, 29]. The power corrections to the evolution have been studied in [30]. Because of the universality of this soft function the non-perturbative corrections that it generates in the TMD-evolution factor are process independent [1, 2, 30].

The soft factor provides finally a rapidity renormalization factor for the jets which is totally analogous to the TMD case, see ref. [31], so that in this sense we can re-write eq. (2.6) as

$$\frac{d\sigma}{de_1 de_2 d\boldsymbol{q}_T} = H_2^{ij}(Q; \mu) \times \mathcal{J}_i^\perp(e_1, Q, z_{\text{cut}}, \boldsymbol{q}_T; \mu, \zeta_A) \otimes \mathcal{J}_j^\perp(e_2, Q, z_{\text{cut}}, \boldsymbol{q}_T; \mu, \zeta_B), \quad (2.8)$$

with $\zeta_A \zeta_B = Q^4 z_{\text{cut}}^4$, which recalls clearly the all-order factorization for the di-hadron fragmentation case using TMD. The hadronization corrections to eq. (2.6)–(2.8) are discussed in more detail in section 4.

The jet-TMD of eq. (2.8) can be re-factorized depending on the relative magnitudes of the effective scales which define it so that one can identify the more complete set of modes

$$\begin{aligned}
\text{soft:} \quad & p_s^\mu \sim q_T(1, 1, 1); \\
\text{collinear:} \quad & p_c^\mu \sim Q(\lambda_c^2, 1, \lambda_c), \ \lambda_c = \sqrt{e}; \\
\text{soft-collinear:} \quad & p_{sc}^\mu \sim Q z_{\text{cut}}(\lambda_{sc}^2, 1, \lambda_{sc}), \ \lambda_{sc} = q_T/(Q z_{\text{cut}}); \\
\text{collinear-soft:} \quad & p_{cs}^\mu \sim Q z_{\text{cut}}(\lambda_{cs}^2, 1, \lambda_{cs}), \ \lambda_{cs} = \sqrt{e/z_{\text{cut}}}
\end{aligned} \quad (2.9)$$

and we illustrate this in figure 3. We start considering the limit $q_T \gtrsim Q\sqrt{e} \gg Q\sqrt{e z_{\text{cut}}}$, which corresponds to region II in figure 3, when the unintegrated and unsubtracted jet function, $\mathcal{J}_i^\perp$, in eq. (2.6) can be re-factorized into three terms,

$$\mathcal{J}_i^\perp(e, Q, z_{\text{cut}}, \boldsymbol{q}_T) = S_{sc,i}^\perp(Q z_{\text{cut}}, \boldsymbol{q}_T) \times \int de' \, S_{cs,i}(e - e', Q z_{\text{cut}}) J_i(e', Q) \quad (2.10)$$

where all the rapidity divergent part and transverse momentum dependence is contained in the calculable $S_{sc,i}^\perp$. The subtracted and unsubtracted jet-TMD are related by

$$\mathcal{J}_i^\perp(e, Q, z_{\text{cut}}, \boldsymbol{b}, \mu, \zeta) = \sqrt{S(\boldsymbol{b})} \mathcal{J}_i^\perp(e, Q, z_{\text{cut}}, \boldsymbol{b}) \quad (2.11)$$

where we have expressed all the subtraction in $\boldsymbol{b}$-space.[3] For smaller values of q_T: $Q \gg Q z_{\text{cut}} \gtrsim Q\sqrt{e} \gg q_T \sim Q\sqrt{e z_{\text{cut}}}$, the collinear-soft and soft-collinear merge into the same mode which we still refer to as collinear-soft. The soft and collinear modes remain unchanged in their scaling compared to region II. The form of factorization theorem in eq. (2.6) does not change but now the corresponding jet TMDs are re-factorized as (see region III in figure 3),

$$\mathcal{J}_i^\perp(e, Q, z_{\text{cut}}, \boldsymbol{q}_T) = \int de' \, S_{cs,i}^\perp(e - e', Q z_{\text{cut}}, \boldsymbol{q}_T) J_i(e', Q). \quad (2.12)$$

---

[3]Throughout the paper we will interchange between $\boldsymbol{q}_T, \boldsymbol{b}$ spaces for the transverse spectrum and between e, s spaces for the jet mass. We use the same symbol for any function in either space. The variable we are working in should be clear from the argument of the function.
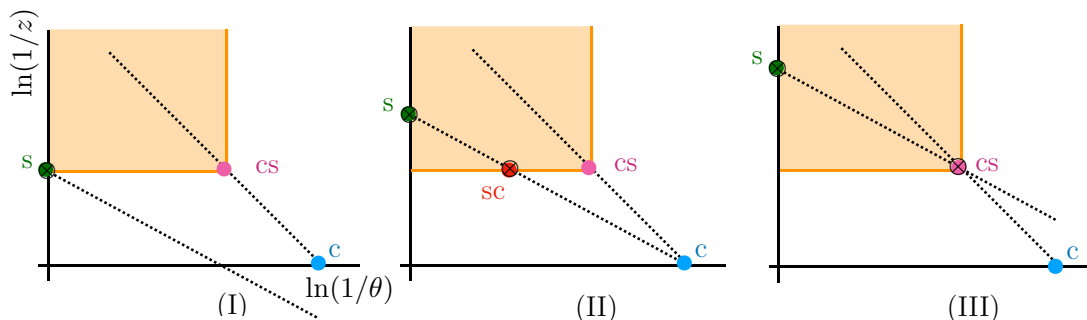
$\otimes$ = contributes to the transverse momentum measurement

Figure 3. Three possible hierarchies for q_T. Shaded region is one that fails Soft-Drop. (I) Largest $q_T \sim Q z_{\rm cut}$. The cross section is factorized into 3 function s, cs and c. (II) The soft function s splits into two s and sc.(III) The sc function merges with the cs function.

Several of the parameters in the differential cross-secion in eq. (2.8) are in practice integrated in experiments, so that it is convenient to explicitly write the cumulant (or partially integrated) distribution

$$\frac{d\sigma}{d\boldsymbol{q}_T}(e_{\rm cut}) = \int_0^{e_{\rm cut}} de_1 de_2 \frac{d\sigma}{de_1 de_2 d\boldsymbol{q}_T}\,. \tag{2.13}$$

For this cross section we work with the integrated jet function which depends on $e_{\rm cut}$ rather than e,

$$\mathcal{J}_j^\perp(e_{\rm cut}, Q, z_{\rm cut}, \boldsymbol{q}_T; \mu, \zeta) = \int_0^{e_{\rm cut}} de\, \mathcal{J}_j^\perp(e, Q, z_{\rm cut}, \boldsymbol{q}_T; \mu, \zeta)\,, \tag{2.14}$$

and the factorization theorem for electron-positron annihilation is

$$\frac{d\sigma}{d\boldsymbol{q}_T}(e_{\rm cut}) = H_2^{ij}(Q; \mu) \int \frac{d\boldsymbol{b}}{4\pi} e^{i\boldsymbol{b}\cdot\boldsymbol{q}_T} \mathcal{J}_i^\perp(e_{\rm cut}, Q, z_{\rm cut}, \boldsymbol{b}; \mu, \zeta) \mathcal{J}_j^\perp(e_{\rm cut}, Q, z_{\rm cut}, \boldsymbol{b}; \mu, \zeta)\,. \tag{2.15}$$

The resummation of logarithms inside the jet-TMD implied by eq. (2.10)–(2.12) is taken into account defining the cumulant jet function as

$$\mathcal{J}_i^\perp(e_{\rm cut}, Q, z_{\rm cut}, \boldsymbol{b}; \mu, \zeta) = \sqrt{S(\boldsymbol{b})} \mathcal{J}_i^\perp(e_{\rm cut}, Q, z_{\rm cut}, \boldsymbol{b})\,, \tag{2.16}$$

$$\mathcal{J}_i^\perp(e_{\rm cut}, Q, z_{\rm cut}, \boldsymbol{b}) = S_{sc,i}^\perp(Q z_{\rm cut}, \boldsymbol{b}) \mathcal{J}_i(e_{\rm cut}, Q, z_{\rm cut}; \mu)\,, \tag{2.17}$$

$$\mathcal{J}_i(e_{\rm cut}, Q, z_{\rm cut}; \mu) = \int_0^{e_{\rm cut}} de \int de'\, S_{cs,i}(e - e', Q, z_{\rm cut}; \mu) J_i(e', Q; \mu) \tag{2.18}$$

and we recall that the rapidity divergences are present only in S and $S_{sc,i}^\perp$, canceling in their product in eq. (2.16). With the exception of the soft-collinear function, $S_{sc}^\perp$, all other ingredients of the factorization are already known at least up to NLO accuracy. In appendix B we report the defining matrix elements of each function, we summarize the NLO results and we perform the NLO calculation of $S_{sc}^\perp$. We have performed the calculation using rapidity regulator. The connection between rapidity regulator and ζ-parameter is outlined in appendix C.2.
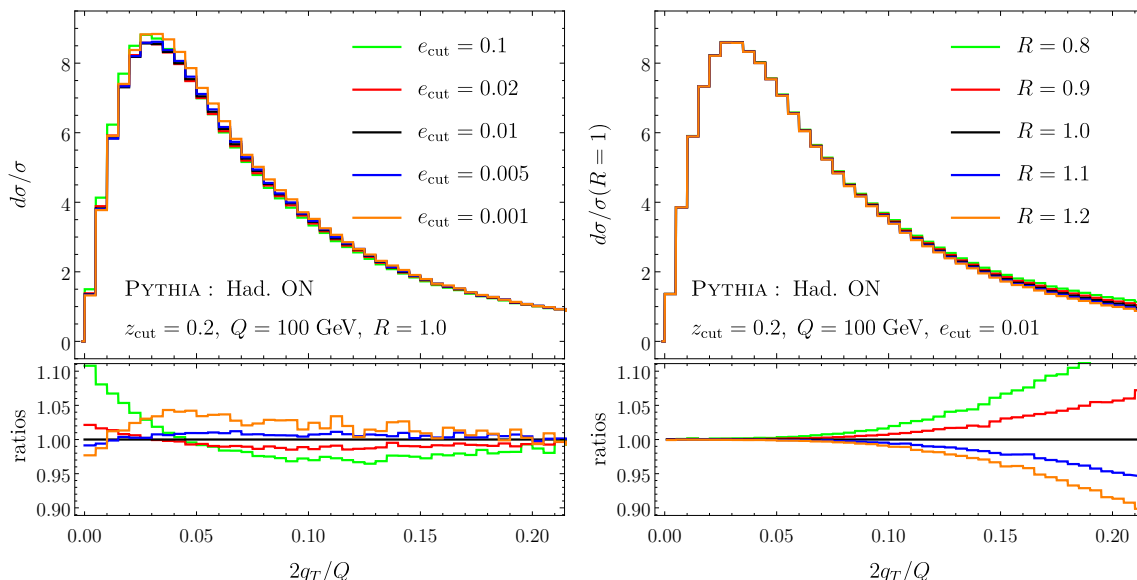
Figure 4. LEFT: The normalized cross sections for different values of the jet mass cutoff parameter $e_{\rm cut}$. We also include the corresponding ratios with respect to the case $e_{\rm cut} = 0.01$. RIGHT: The *relatively* normalized cross section for fixed $e_{\rm cut} = 0.01$ and for different value of the jet radius R. The corresponding ratios are with respect to $R = 1$.

Finally we observe that using monte-carlo simulations (particularly PYTHIA 8 [13, 14]) most of the events fall in the kinematic regime

$$Q \gg Q z_{\rm cut} \gg q_T \sim Q\sqrt{e_{\rm cut}}\,. \tag{2.19}$$

An important consequence of the jet function refactorization in eq. (2.10) is that the transverse momentum dependent elements decouple from the jet mass elements. This suggests that, as long as we remain within the hierarchy of eq. (2.19), then the exact mass cutoff on the invariant mass will only influence the overall normalization and not the shape of the TMD distribution. We test this observation against the monte-carlo simulations by comparing the normalized TMD distributions for various values of $e_{\rm cut}$. We show the results in figure 4 (left). The jet algorithm is implemented through FASTJET-3 [32]. In addition we note that as long as we measure $q_T \ll Q z_{\rm cut}$ and for $R \sim 1$ the shape and normalization of the cross section is independent of the choice of R. We also demonstrate this with the help of simulations. We simulate events at $Q = 50\,{\rm GeV}$ and we analyze them for different values of $R \gtrsim 1$. We show the resulting distributions in figure 4 (right). Note that for that plot we preserve the relative normalizations of the curves.

2.3 Renormalization group evolution

The two main quantities involved in the factorization procedure carried out in previous section are the subtracted jet-TMD for which we have

$$\mu\frac{d}{d\mu}\mathcal{J}^{\perp}(e, Q, z_{\rm cut}, \boldsymbol{b}, \mu, \zeta) = \gamma_F^q(\mu, \zeta)\mathcal{J}^{\perp}(e, Q, z_{\rm cut}, \boldsymbol{b}, \mu, \zeta), \tag{2.20}$$

$$\zeta\frac{d}{d\zeta}\mathcal{J}^{\perp}(e, Q, z_{\rm cut}, \boldsymbol{b}, \mu, \zeta) = -\mathcal{D}^q(\mu, \boldsymbol{b})\mathcal{J}^{\perp}(e, Q, z_{\rm cut}, \boldsymbol{b}, \mu, \zeta), \tag{2.21}$$

where on the r.h.s. we have considered just quark initiated jets and we have Fourier transformed with respect to $\boldsymbol{q}_T$ the jet functions appearing in eq. (2.8). Of course this result recalls literally the standard TMD case.

However, because of the re-factorization of $\mathcal{J}^\perp$ (see eq. (2.10)–(2.12)) this resummation is not complete and large logarithms can still spoil the convergence of the perturbative series. Defining s as the variable conjugate to e in Laplace space (see appendix A) and

$$G \in \left\{ S_{sc}^{sub}(Qz_{\text{cut}}, \boldsymbol{b}),\ S_{cs}(s, Qz_{\text{cut}}),\ J(s, Q) \right\};\quad S_{sc}^{sub}(Qz_{\text{cut}}, \boldsymbol{b}) = \sqrt{S(\boldsymbol{b})}S_{sc}(Qz_{\text{cut}}, \boldsymbol{b}),\tag{2.22}$$

we have

$$\mu\frac{d}{d\mu}G = \gamma^G(\mu, \alpha_s)G = \left(\Gamma^G[\alpha_S]\mathbf{l}_{m_G^2} + \Delta\gamma^G[\alpha_S]\right)G,\tag{2.23}$$

which are formally similar to the TMD case and the values of m_G are reported in the appendix in table 1. The only function in G which has a rapidity evolution equation is S_{sc}^{sub} and it scales like $\mathcal{J}^\perp$ in eq. (2.21). The cusp part of eq. (2.23) is proportional to the standard cusp anomalous dimension

$$\Gamma_\mu^G[\alpha_s] = \frac{\Gamma_0^G}{\Gamma_0^{\text{cusp}}}\Gamma^{\text{cusp}} = \frac{\Gamma_0^G}{\Gamma_0^{\text{cusp}}}\sum_{n=0}^{\infty}\left(\frac{\alpha_s}{4\pi}\right)^{1+n}\Gamma_n^{\text{cusp}}.\tag{2.24}$$

For the non-cusp part we have also a perturbative expansion

$$\Delta\gamma^G[\alpha_S] = \sum_{n=0}^{\infty}\left(\frac{\alpha_s}{4\pi}\right)^{1+n}\gamma_n^G.\tag{2.25}$$

The anomalous dimensions that enter in the calculations for each case are given in appendix C. The evolution in rapidity and factorization scales of all quantities can be implemented using the ζ-prescription whose general framework can be found in ref. [33]. We provide some details for the present case in the appendix.

The resummation of potentially large logarithms inside the jet-TMD is done performing the evolution in Laplace space and then integrating such that we get the cumulant before we take the inverse transform. In this way we resum logarithms which are associated to e_{cut}. All this works as follows. Starting from eq. (2.18), then taking the Laplace and consecutively the inverse transform with respect to e we find

$$\mathcal{J}_i(e_{\text{cut}}, Q, z_{\text{cut}}; \mu) = \frac{1}{2\pi i}\int_{\gamma-i\infty}^{\gamma+i\infty} ds\frac{\exp(se_{\text{cut}}) - 1}{s}S_{cs,i}(s, Q, z_{\text{cut}}; \mu)J_i(s, Q; \mu).\tag{2.26}$$

Then solving the RGE equations for the collinear-soft and jet function as described in appendix C.1, and performing the last remaining integral over the Laplace conjugate variable s we get

$$\mathcal{J}_i(e_{\text{cut}}, Q, z_{\text{cut}}; \mu) = \exp\left(K_{cs}(\mu, \mu_{cs}) + K_J(\mu, \mu_J)\right)S_{cs,i}(L_{cs} \to \partial_{\omega_{cs}}; \mu_{cs})J_i(L_J \to \partial_{\omega_J}; \mu_J)$$

$$\left(\frac{\mu_{cs}}{Q\sqrt{z_{\text{cut}}e_{\text{cut}}}}\right)^{2\omega_{cs}(\mu, \mu_{cs})}\left(\frac{\mu_J}{Q\sqrt{e_{\text{cut}}}}\right)^{2\omega_J(\mu, \mu_J)}\frac{\exp(\gamma_E(\omega_{cs}(\mu, \mu_{cs}) + \omega_J(\mu, \mu_J)))}{\Gamma(1 - \omega_{cs}(\mu, \mu_{cs}) - \omega_J(\mu, \mu_J))}.\tag{2.27}$$

This is our final result for the resummed cumulant jet function. The order of logarithmic accuracy is then determined by the order of which the kernels K_F, ω_F, and the fixed order collinear-soft and jet functions are evaluated. At this stage of the calculation the canonical scales, μ_{cs} and μ_J, are not yet fixed. This allows us to choose the scales such that potentially large logarithms are minimized in momentum space. From the above is clear that the canonical choice of scales such as the fixed order logarithms are minimized are,

$$\mu_{cs} = Q\sqrt{z_{\text{cut}}e_{\text{cut}}}\,, \qquad\qquad \mu_J = Q\sqrt{e_{\text{cut}}}\,. \qquad (2.28)$$

In numerical applications one needs to perform variations around these scales in order to obtain an estimate of the theoretical uncertainty.

2.4 Numerical results for e^+e^-

In this section, we provide the results of our calculation for $e^+e^- \to 2$ jets computed up to NNLL accuracy. The implementation necessarily needs a choice for the rapidity scales and we have done it using the ζ-prescription as described in ref. [33] and adapting the code `artemide` to the present case. This consisted of performing the evolution of the transverse momentum dependent components within the `artemide` framework, while for all other scales not involved in the rapidity evolution, i.e., the hard and jet functions, see appendix C.1.

There are some important modifications to the ζ-prescription framework for our case which affect the numerics. One of this is that now $\zeta_A\zeta_B \sim Q^4 z_{\text{cut}}^4$ compared to the di-hadron decorrelation case where $\zeta_A\zeta_B \sim Q^4$. This means that the effective hard scale to which the distributions are sensitive is lower. Because the TMD factorization is valid when q_T is much lower than the hard scale of the process, one needs that the product Qz_{cut} be sufficiently high. In our plots we have considered the case $q_T \lesssim Qz_{\text{cut}}$. Then the evolution of the jet-TMD given in eq. (2.23) is also slightly different from the standard hadron TMD, although the changes are implemented easily in the `artemide` code. A one-loop check of all anomalous dimensions is provided in appendix B.

In figure 5 we compare our analytic result for NLL cross section (normalized) against PYTHIA simulations for $Q = 50$ and $100\,\text{GeV}$. For the purposes of comparison we turn hadronization off in the simulation and we compare against our purely perturbative result. The perturbative calculation depends on the parameter B_{NP} which in practice implements a cutoff in the inverse Laplace transform such that the soft scale, that behaves as $1/b$, does not hit the Landau pole. As long as we choose this parameter such that convergence of the integral is reached before the cutoff, then the perturbative result is not much sensitive to the value of B_{NP}. Although, as we now discuss, the theoretical uncertainty of the cross section for these energies at NLL is quite large, we find very good agreement with the simulations for the canonical choice of scales (i.e., central line in figure 5).

In figure 6 we give the NNLL results including a theoretical uncertainty band. We compare against the NLL cross section and although the error bands seem to be larger than what is typically expected we can clearly see that the result convergences and the theory error decreases by approximately factor of two. To estimate the theoretical uncertainty we
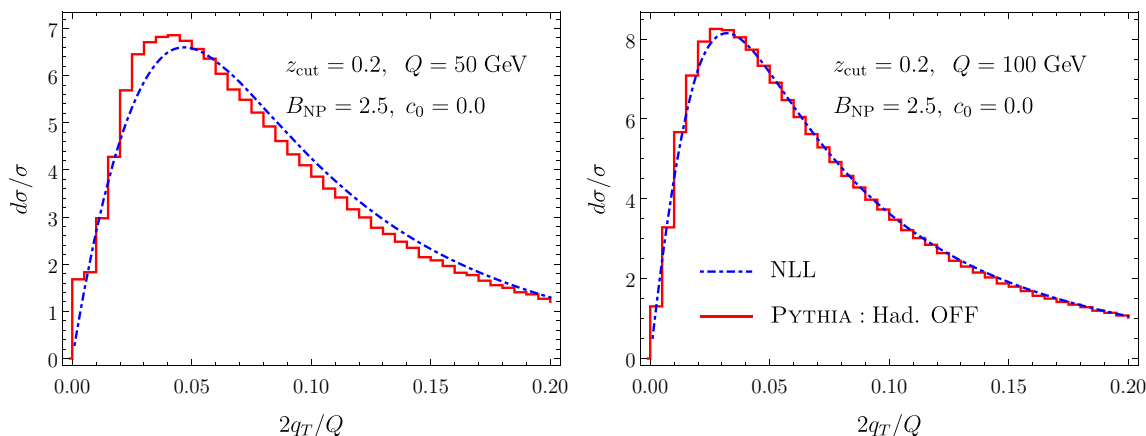
Figure 5. Comparison of the NLL result against the partonic shower of PYTHIA 8 for $R = 1$ and $e_{\text{cut}} = 0.01$ for two different center of mass energies, LEFT: $50\,\text{GeV}$, RIGHT: $100\,\text{GeV}$.
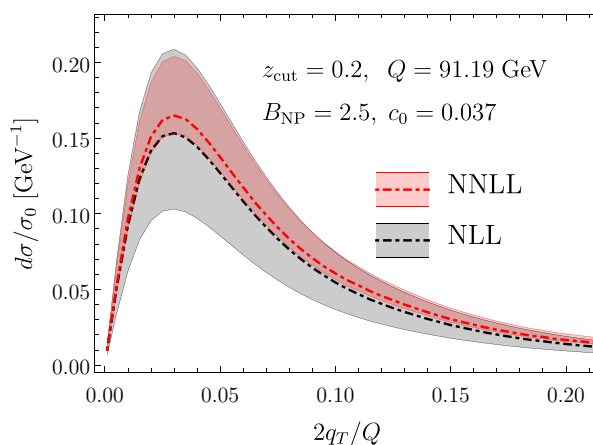
Figure 6. Transverse momentum de-correlation for $e^+e^- \rightarrow$ dijets with center of mass energy at the Z mass.

first vary all the factorization scales of a factor 2 (0.5) around their canonical value, then we separately take the envelope of the variations involved in rapidity evolution, μ, μ_{sc}, and of the ones involved only in the virtuality evolution of the jet function, μ_{cs}, μ_J. The final error bands we show are the quadrature of the two contributions. The reason for this prescription is that rapidity and virtuality evolutions are in principle uncorrelated. The uncertainty is somewhat larger than what one might expect for a NNLL calculation, and is practically dominated by the variations in the jet function. This is attributed to the small values of the collinear-soft scale, $\mu_{cs} \sim Q\sqrt{e_{\text{cut}}z_{\text{cut}}}$, which approaches the non-perturbative regime even for values of $Q \sim m_Z$. One might attempt to reduce the uncertainty by increasing either e_{cut} or z_{cut}, but caution is needed not to invalidate the corresponding hierarchy. We will see later that when only the mass of one jet is measured (e.g., in DIS or hadron-jet decorrelation) then the error band decreases significantly.

3 Jets in DIS

The advent of new colliders like EIC and LHeC makes the measurement of jets interesting also in semi-inclusive deep inelastic scattering (SIDIS) experiments. Actually we want to explore the possibility of using jets to study the TMDPDF.

For the present case we demand that the hard scattering of the lepton on the proton produces a single jet. In the Breit frame we measure the transverse component, $\boldsymbol{q}_T$, of the transferred momentum, $q^\mu = k'^\mu - k^\mu$ with respect to the single groomed jet. As before, we impose a jet mass cut-off e_{cut} and the grooming parameter z_{cut}. In this framework the initial state proton is moving along the $-z$ direction and the final state jet is moving in the opposite $+z$-direction, so that we can assign the directions n and $\bar{n}$ to the beam and jet definition. The contribution to this transverse momentum measurement comes from the initial state radiation which forms part of the TMDPDF and the radiation that fails soft-drop in the final state jet. We demand that there is a single energetic jet with $E_J \sim Q/2 = \sqrt{-q^2}/2$ with accompanying soft radiation.

It is instructive to setup some of the notation that we are using for describing the kinematics in the Breit frame. The virtual photon is assumed to be completely space-like and it has only the z component of the momentum. Defining our light-cone directions $n^\mu = (1, 0, 0, +1)$ and $\bar{n}^\mu = (1, 0, 0, -1)$, the resulting photon momentum q^μ is

$$q^\mu = \frac{Q}{2}(n^\mu - \bar{n}^\mu), \qquad (3.1)$$

where $Q^2 = -q^2$ is a positive quantity. We assume that at the partonic level, a single quark carrying x fraction of the proton longitudinal momentum undergoes a hard interaction with the virtual photon. In this frame, the proton is moving along the $-z$ direction and its momentum can be written as:

$$P^\mu = \frac{Q}{2x}\bar{n}^\mu. \qquad (3.2)$$

At tree level and by momentum conservation the final state parton will carry momentum

$$xP^\mu + q^\mu = \frac{Q}{2}(n^\mu - \bar{n}^\mu) + \frac{Q}{2}\bar{n}^\mu = \frac{Q}{2}n^\mu, \qquad (3.3)$$

which is exactly opposite in direction to the incoming beam. Of course this will be modified beyond tree-level when initial and final state radiation is included.

3.1 Schematics for factorization

Since we are working with two back-to-back directions, our usual definition of the soft function holds: in other words the change from future pointing to past pointing Wilson lines does not affect its value [1–5].

Since we still impose the same jet mass measurement on the final state jet, we have all the modes that we had in the e^+e^- case. The main difference is that now the initial hadronic state is a TMDPDF. The form of the factorized cross section follows again the hierarchy $Q \gg Qz_{\text{cut}} \gg q_T$, $R \sim 1$ and

$$\frac{d\sigma}{dx dQ^2 d\boldsymbol{q}_T} = \mathcal{N}(x, Q)H_2(Q, \mu) \times S(\boldsymbol{q}_T) \otimes B_{i \leftarrow h}(x, Q, \boldsymbol{q}_T) \otimes \mathcal{J}_j^\perp(e_{\text{cut}}, Q, z_{\text{cut}}, \boldsymbol{q}_T), \quad (3.4)$$

where $x = -q^2/(2P \cdot k)$, k is the momentum of the incoming electron, and $\mathcal{N}(x, Q)$ is the over-all normalization which we give later in this section. The un-subtracted TMDPDF is $B_{i \leftarrow h}$. In our rapidity regularization scheme the (subtracted) TMDPDF is defined as

$$F_{i \leftarrow h}(x, \boldsymbol{b}; \mu, \zeta) = \sqrt{S(\boldsymbol{b})} B_{i \leftarrow h}(x, Q, \boldsymbol{b}). \tag{3.5}$$

At perturbative values of q_T, the $F_{i \leftarrow h}$ can be matched onto the collinear PDF. The matching coefficients at NNLO are evaluated in [31, 34] and in the appendix we review some one-loop results. Once the subtracted quantities are included we can write

$$\frac{d\sigma}{dx dQ^2 d\boldsymbol{q}_T} = \mathcal{N}(x, Q) H_2(Q, \mu) \int \frac{d\boldsymbol{b}}{4\pi^2} e^{i\boldsymbol{b} \cdot \boldsymbol{q}_T} F_{i \leftarrow h}(x, Q, \boldsymbol{b}, \mu, \zeta_A) \mathcal{J}_j^\perp(e_{\text{cut}}, Q, z_{\text{cut}}, \boldsymbol{b}; \mu, \zeta_B). \tag{3.6}$$

The evolution under renormalization group equations for the TMDPDF is widely known (see e.g. [33, 35–37]) and we recall a few characteristics here. One has

$$\mu \frac{d}{d\mu} F_{f \leftarrow f'}(x, \boldsymbol{b}, \mu, \zeta) = \gamma_F^f(\mu, \zeta) F_{f \leftarrow f'}(x, \boldsymbol{b}, \mu, \zeta),$$

$$\zeta \frac{d}{d\zeta} F_{f \leftarrow f'}(x, \boldsymbol{b}, \mu, \zeta) = -\mathcal{D}^f(\mu, \boldsymbol{b}) F_{f \leftarrow f'}(x, \boldsymbol{b}, \mu, \zeta), \tag{3.7}$$

where $\mathcal{D}_f$ and γ_F^f are the rapidity and UV anomalous dimensions, respectively. The integrability requirement of this couple of equation results in

$$\mu \frac{d}{d\mu} \left(-\mathcal{D}^f(\mu, \boldsymbol{b}) \right) = \zeta \frac{d}{d\zeta} \gamma_F^f(\mu, \zeta) = -\Gamma_f^{\text{cusp}} \tag{3.8}$$

where Γ_f^{cusp} is the cusp anomalous dimension. The UV anomalous dimension is written in these terms as

$$\gamma_F^f = \Gamma_f^{\text{cusp}} \mathbf{l}_\zeta - \gamma_V^f, \tag{3.9}$$

γ_V^f being the non-cusp part of the anomalous dimension and $\mathbf{l}_\zeta = \ln \left(\mu^2/\zeta \right)$. The γ_V and $\mathcal{D}$ anomalous dimensions are known up to $\mathcal{O}(a_s^3)$ [28, 29, 38–40]. A numerical calculation for the four-loop cusp anomalous dimension was recently given in [41]. All the evolution equations are the same for the case of TMD fragmentation functions, and we do not discuss them any more here.

3.2 Derivation of the factorized cross section using jets

In this section we provide some details for the factorization of the SIDIS cross section in eq. (3.4), (3.6). The scattering amplitude for the process $ep \to ef$ where f is the final state is given by:

$$iM(ep \to ef) = (-ie^2) \bar{u}(k') \gamma_\mu u(k) \frac{1}{q^2} \langle f | J^\mu(0) | p(P) \rangle, \tag{3.10}$$

and thus the corresponding cross section is given by

$$d\sigma(ep \to ef) = \frac{e^4}{4(s-m^2)} \int \frac{d^3k'}{2(2\pi)^3 E_{k'}} \, \text{tr}\Big[\not{k}\gamma_\mu \not{k}'\gamma_\nu\Big]$$
$$\sum_f \int d\Pi_f \, \langle p(P)|J^{\dagger\mu}(0)|f\rangle\langle f|J^\nu(0)|p(P)\rangle (2\pi)^4\delta^{(4)}(q+P-p_f)\,, \quad (3.11)$$

where $q = k' - k$. We can use the standard parametrization of the final electron phase-space to write:

$$\int \frac{d^3k'}{2(2\pi)^3 E_{k'}} = dx dy \frac{ys}{(4\pi)^2}\,, \quad (3.12)$$

where $y = (2P\cdot q)/(2P\cdot k)$ and s is the hadronic Mandelstam variable. We then get,

$$\frac{d\sigma}{dxdy}(ep \to ef) = L_{\mu\nu}(k,k') \sum_f \int d^4r e^{iq\cdot r} \int d\Pi_f \, \langle p(P)|J^{\dagger\mu}(0)|f\rangle\langle f|J^\nu(x)|p(P)\rangle\,, \quad (3.13)$$

where r^μ is Fourier conjugate of the momenta q^μ and $L^{\mu\nu}$ is the leptonic tensor,

$$L_{\mu\nu}(k,k') \equiv \frac{\alpha^2 ys}{4(s-m^2)}\text{tr}\Big[\not{k}\gamma_\mu \not{k}'\gamma_\nu\Big]\,. \quad (3.14)$$

The next step is to project the hadronic final state $|f\rangle$ onto the one that corresponds to the measurement that we are proposing, i.e.,

$$\int d\Pi_f |f\rangle\langle f| \;\to\; \int d\boldsymbol{q}_T z dz \int d\Pi_{f[\text{g-jet}(z\boldsymbol{q}_T,z)]}|f\rangle\langle f|\,. \quad (3.15)$$

We can now match the full theory hadronic current $J_\mu(x)$ onto the SCET$_+$ [42] current working in the Breit frame,

$$J^\mu(x) = C^{\mu\nu}(Q)\Big[\bar{\chi}_{n,Q} S_n^\dagger W_t^\dagger U_n \gamma_\nu S_{\bar{n}} \chi_{\bar{n},Q}\Big] + \mathcal{O}(\lambda)\,, \quad (3.16)$$

where λ is the power counting parameter of our EFT which will turn out to be $q_\perp/Q \sim e_{\text{cut}}/Q$. Note that in the same step, through BPS field redefinition, we decoupled the collinear soft modes from the collinear modes and hence the presence of the U_n Wilson lines. In the matching we also have the soft Wilson lines S_n. From the kinematic constraints of the measurement and since all the modes that are present in the projected final state are decoupled from each other at the level of the Lagrangian, (we assume that contributions from Glauber gluon exchanges cancel) it is possible to factorize the final state as follows,

$$|f\rangle \;\to\; |X_{\bar{n}}\rangle|X_n\rangle|X_s\rangle|X_{sc}\rangle\,, \quad (3.17)$$

where we have included in X_n all possible modes that contribute to the invariant mass measurement. Refactorization of the n-collinear sector follows from the same steps as in the case of electron-positron annihilation presented in ref. [43]. We are now ready to factorize the cross section into individual SCET matrix elements. In the final result one needs to be careful regarding all the index contractions and the tensor structures. This was

carefully considered in ref. [44]. In addition we are considering the case where the frame we are working is rotated such that the transverse momentum of the groomed jet is zero. After all rearrangements we get,

$$\frac{d\sigma}{dxdydzd\boldsymbol{q}_T}(ep \to ef) = \sigma_0(x,Q) \times H_2(Q) \int d^4r e^{iq \cdot r}$$
$$\frac{1}{N_c} \sum_{X_s} \langle 0|S_n S_{\bar{n}}^\dagger(r_\perp)|X_s\rangle\langle X_s|S_{\bar{n}} S_n^\dagger(0)|0\rangle$$
$$\times \sum_{X_{\bar{n}}} \langle p(P)|\bar{\chi}_{\bar{n}}(r^+, r_\perp)\frac{\gamma^+}{2}|X_{\bar{n}}\rangle\langle X_{\bar{n}}|\chi_{\bar{n}}(0)|p(P)\rangle \qquad (3.18)$$
$$\times \frac{1}{N_c} \sum_{X_{sc}} \langle 0|U_n^\dagger W_t(r_\perp)|X_{sc}\rangle\langle X_{sc}|W_t^\dagger U_n(0)|0\rangle$$
$$\times \frac{z}{2N_c}\mathrm{tr} \sum_{X_n} \langle 0|\frac{\gamma^-}{2}\chi_n(r^-, r_\perp)|X_n\rangle\langle X_n|\bar{\chi}_n(0)|0\rangle|_{p_\perp^{X_n}=0}.$$

The hard matching coefficient in general has two Lorentz structures, given the two types of currents, vector and axial. For the case of photon with vector current, we simply have $H^{\mu\nu} \sim g_\perp^{\mu\nu}$. We have also multipole-expanded the final result. To proceed with the factorization theorem in momentum space, we remove $r_\perp$ dependence from the various EFT matrix elements by acting the corresponding fields on the final states. This gives us

$$\frac{d\sigma}{dxdydzd\boldsymbol{q}_T}(ep \to ef) = \sigma_0(x,Q) \times H_2(Q) \int d^4r e^{iq \cdot r + i\left(\boldsymbol{p}_\perp^{X_{\bar{n}}^R} + \boldsymbol{p}_\perp^S\right) \cdot \boldsymbol{r}_\perp}$$
$$\frac{1}{N_c} \sum_{X_s} \langle 0|S_n S_{\bar{n}}^\dagger(0)|X_s\rangle\langle X_s|S_{\bar{n}} S_n^\dagger(0)|0\rangle$$
$$\times \sum_{X_{\bar{n}}} \langle p(P)|\bar{\chi}_{\bar{n}}(r^+, 0_\perp)\frac{\gamma^+}{2}|X_{\bar{n}}\rangle\langle X_{\bar{n}}|\chi_{\bar{n}}(0)|p(P)\rangle \qquad (3.19)$$
$$\times \frac{1}{N_c} \sum_{X_{sc}} \langle 0|U_n^\dagger W_t(0)|X_{sc}\rangle\langle X_{sc}|W_t^\dagger U_n(0)|0\rangle$$
$$\times \frac{z}{2N_c}\mathrm{tr} \sum_{X_n} \langle 0|\frac{\gamma^-}{2}\chi_n(r^-, 0_\perp)|X_n\rangle\langle X_n|\bar{\chi}_n(0)|0\rangle|_{p_\perp^{X_n}=0},$$

where

$$p_\perp^{X_{\bar{n}}^R}\big|_{p_\perp^{\text{g-jet}}=0} = p_\perp^{X_{\bar{n}}} - P_\perp\big|_{p_\perp^{\text{g-jet}}=0} = p_\perp^{X_{\bar{n}}}\big|_{P_\perp=0}\Big(1 + \mathcal{O}(\lambda)\Big), \qquad (3.20)$$

is the difference in the transverse momentum of the recoiling initial state collinear radiation and the proton with respect to the hadrons direction, which up to power-corrections of order $\mathcal{O}(\lambda)$ is simply the transverse momentum of the recoiling radiation with respect to

the proton. Performing the integral over d^4r we get:

$$\frac{d\sigma}{dxdydzd\boldsymbol{q}_T}(ep \to ef) = \sigma_0(x,Q) \times H_2(Q)\delta^{(2)}\left(\boldsymbol{q}_T + \boldsymbol{p}_\perp^{X_{\bar{n}}^R} + \boldsymbol{p}_\perp^{X_s} + \boldsymbol{p}_\perp^{X_{sc}}\right)$$

$$\frac{1}{N_c}\sum_{X_s}\langle 0|S_n S_{\bar{n}}^\dagger(0)|X_s\rangle\langle X_s|S_{\bar{n}}S_n^\dagger(0)|0\rangle$$

$$\times \sum_{X_{\bar{n}}}\langle p(P)|\bar{\chi}_{\bar{n}}(0)\frac{\gamma^+}{2}\delta(q^- - p_{X_{\bar{n}}}^-)|X_{\bar{n}}\rangle\langle X_{\bar{n}}|\chi_{\bar{n}}(0)|p(P)\rangle \quad (3.21)$$

$$\times \frac{1}{N_c}\sum_{X_{sc}}\langle 0|U_n^\dagger W_t(0)|X_{sc}\rangle\langle X_{sc}|W_t^\dagger U_n(0)|0\rangle$$

$$\times \frac{z}{2N_c}\operatorname{tr}\sum_{X_n}\langle 0|\frac{\gamma^-}{2}\chi_n(0)\delta(q^+ - p_{X_n}^+)|X_n\rangle\langle X_n|\bar{\chi}_n(0)|0\rangle|_{p_\perp^{X_n}=0}\,.$$

In order to simplify our result further we introduce "measurement" delta functions for the soft and initial state matrix elements. This will allow us to absorb the $p_\perp^{X_i}$ into the corresponding matrix elements and use

$$\mathbf{1}_i = \sum_{X_i}|X_i\rangle\langle X_i|\,, \quad (3.22)$$

to further simplify the form of EFT matrix elements. We also perform a type-I RPI transformation in order to rewrite the proton matrix elements as function of fields with respect to the initial state proton axis. We thus get

$$\frac{d\sigma}{dxdydzd\boldsymbol{q}_T}(ep \to ef) = \sigma_0(x,Q) \times H_2(Q)\int d\boldsymbol{p}_\perp^s d\boldsymbol{p}_\perp^{sc} d\boldsymbol{p}_\perp^c \,\delta^{(2)}(\boldsymbol{q}_T + \boldsymbol{p}_\perp^c + \boldsymbol{p}_\perp^s + \boldsymbol{p}_\perp^{sc})$$

$$\frac{1}{N_c}\langle 0|T\left(S_n S_{\bar{n}}^\dagger(0)\right)\delta^{(2)}(\boldsymbol{p}_\perp^s - \boldsymbol{\mathcal{P}}_\perp)\bar{T}\left(S_{\bar{n}}S_n^\dagger(0)\right)|0\rangle$$

$$\times \langle p(P)|\bar{\chi}_{\bar{n}}(0)\frac{\gamma^+}{2}\delta(q^- - \mathcal{P}^-)\delta^{(2)}(\boldsymbol{p}_\perp^c - \boldsymbol{\mathcal{P}}_\perp)\chi_{\bar{n}}(0)|p(P)\rangle|_{P_\perp=0}$$

$$\times \frac{1}{N_c}\langle 0|T\left(U_n^\dagger W_t(0)\right)\mathcal{M}_\perp^{\mathrm{SD}}\bar{T}\left(W_t^\dagger U_n(0)\right)|0\rangle \quad (3.23)$$

$$\times \frac{z}{2N_c}\operatorname{tr}\sum_{X_n}\langle 0|\frac{\gamma^-}{2}\chi_n(0)\delta(q^+ - \mathcal{P}^+)|X_n\rangle\langle X_n|\bar{\chi}_n(0)|0\rangle|_{p_\perp^{X_n}=0}\,,$$

where $\mathcal{M}_\perp^{\mathrm{SD}}$ is the measurement function given in eq. (B.26). Since we are considering only large radius jets with $R \gtrsim 1$ we may trivially perform the integration of the energy fraction z using $Q \simeq p_+^{X_n}$ up to power corrections. Also performing change of integration variables,

$$dxdy = \frac{dxdQ^2}{xs}\,, \quad (3.24)$$

we get eq. (3.4) with

$$\mathcal{N}(x,Q) = \frac{\sigma_0(x,Q)}{xs}\,, \quad (3.25)$$

and the matrix elements involved in the functions S, B, and $\mathcal{J}$ are given in the appendix. For the case of groomed jets with invariant mass cutoff it is possible to refactorize the jet
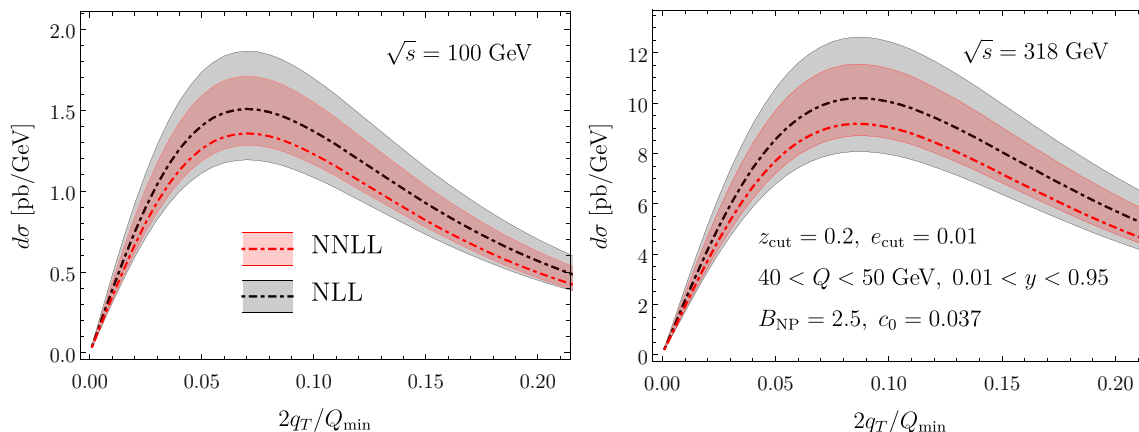
Figure 7. The NLL and NNLL TMD spectra for groomed jets in DIS for EIC (left: $\sqrt{100}\,\text{GeV}$) and HERA (right: $\sqrt{s} = 318\,\text{GeV}$) kinematics. The cross section are integrated in $y = Q^2/(xs)$ and $Q = \sqrt{-q^2}$ (see details in the main text).

function. This is done in ref. [43] and thus we do not demonstrate it here. Then integrating over $e \in (0, e_{\text{cut}})$ gives the dependence of the jet function in the parameter e_{cut}. This is identical to the analysis in the previous section on e^+e^-. This is our final result for the factorization theorem in DIS.

3.3 Numerical results for DIS

In this section we use the factorization theorem in eq. (3.4) to obtain numerical results for the TMD spectrum of groomed jets in DIS process. Our analysis is done for two center-of-mass energies, EIC: $\sqrt{s} = 100\,\text{GeV}$ and HERA: $318\,\text{GeV}$. For both energies we integrate over $y = Q^2/(xs)$ and $Q = \sqrt{-q^2}$ in the regions $0.01 < y < 0.95$ and $40 < Q < 50\,\text{GeV}$. For the TMDPDFs we use the fits obtained from Drell-Yan data [45] with the use of ζ-prescription. In figure 7 we show our results for NLL and NNLL accuracies for the two center of mass choices, including theoretical uncertainties. We estimate the theoretical scale variations as described in section 2.4. The groomed jet parameters that we choose are the same as in the di-lepton case: $\beta = 0$, $z_{\text{cut}} = 0.2$, and $e_{\text{cut}} = 0.01$. As before we find good convergence between the NLL and NNLL result. The absolute value of theoretical scale variation is improvable with higher logarithmic accuracy (NNLL-prime or perhaps N^{3}LL), which needs the explicit calculation of several jet hadronic matrix elements at two loops.

We further investigate the size of the uncertainty due to the hadronic initial state and the non-perturbative effects induced by TMD evolution. We do that by varying the model parameters as constrained by the phenomenological analysis in ref. [45] for our NNLL result. The results are shown in figure 8. We consider both variable and fixed $B_{\text{NP}} = 2.5\,\text{GeV}^{-1}$ (for details on the difference of the two schemes see [45]). We find that the effects (for our kinematics) are particularly small, of the order of $\sim 5\%$, which is much smaller than the theoretical uncertainties. This suggests that we need a better control over the theoretical uncertainties in order to further constrain TMD distributions from groomed jets in DIS. As mentioned earlier the uncertainty can be mitigated with higher logarithmic accuracy
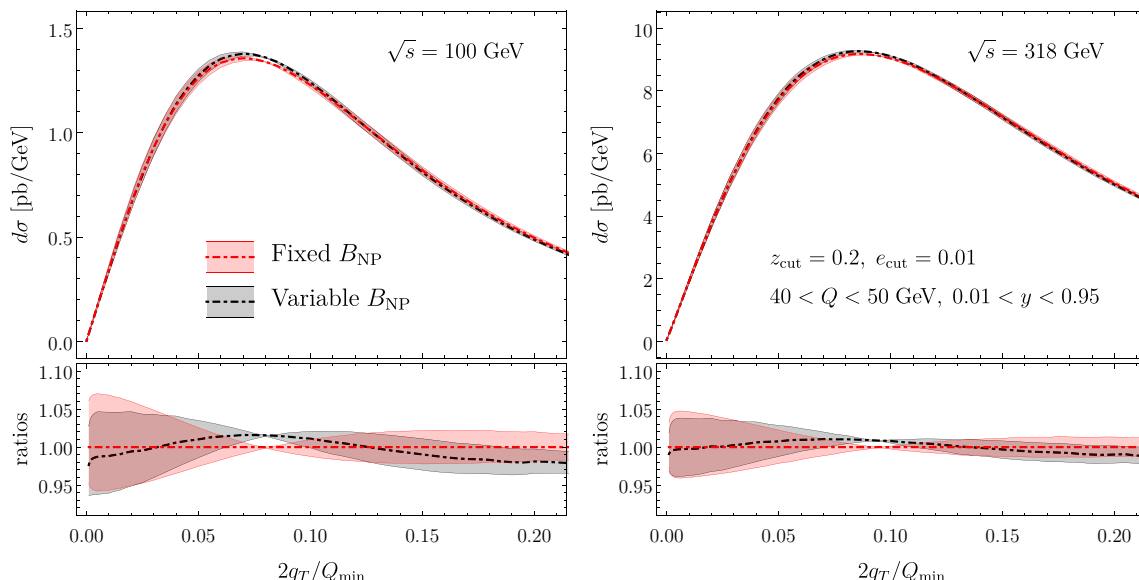
Figure 8. The NNLL cross-section including modeling of the initial hadronic state effects fitted from Derll-Yan processes using two different scenes: fixed and variable B_{NP}.

or by choosing larger values of e_{cut}, still compatible with factorization. This, will require to treat the region III shown in figure 3. For this reason it is interesting to investigate the range of values of e_{cut} for which the energetic wide angle radiation is avoided.

4 Hadronization effects

One of the goals of the paper is to study the non-perturbative effects associated with TMD distributions, in this case the TMDPDF. Usually in any experiment, there are multiple sources of non-perturbative corrections associated with both the initial and final states. To have access to a specific source of corrections, its therefore necessary to separate out the pieces of interest from the uninteresting ones, which in this case constitute the final state hadronization corrections. To access the TMD then, we must already have a good extraction of the rest of the non-perturbative effects. This is the reason why we consider distinct experiments in this paper. The idea, as we shall demonstrate, is that the final state hadronization corrections are exactly the same in the two experiments. The $e^+e^- \to 2$ jets case can be used to extract out all the final state hadronization corrections, which can then be used for DIS.

For the e^+e^- observable, the factorization takes the form in eq. (2.8), we can then study the non-perturbative corrections for each collinear object $\mathcal{J}_i^\perp$, which by symmetry, are the same for the two objects. If we now look at the factorization for DIS, eq. (3.6), the key point to note is that $\mathcal{J}_j^\perp(e_{\mathrm{cut}}, Q, z_{\mathrm{cut}}, \boldsymbol{b}; \mu, \zeta_B)$ is the same object that appears in the case of e^+e^-, while $F_{i\leftarrow h}$ is just the TMDPDF. Thus it now becomes possible to exclusively access the complete TMDPDF. We now wish to systematically list the sources of the non-perturbative corrections associated with each factorized function that appear in our cross section.

In order to use jets it is important to consider all the non-perturbative effects for the case of our observables and in particular the ones coming from the implementation of (groomed) jets. In figure 1 we have shown that such corrections are expected to be particularly small and we provide here a discussion about their origin from a theory perspective. We have two measurements on the jet: the jet mass, which is ultimately integrated over some interval and acts as a normalization, and the transverse momentum $(p_\perp)$ of the radiation that is groomed away. Since we are interested in the shape of the q_T spectrum, we will only consider the non-perturbative effects in cross sections sensitive to it. As was explained in section 2, we are working in the region II of EFT and we are going to discuss how non-perturbative effect arise when we increase the value of q_T (that is, we discuss here the non-perturbative corrections in the small-b limit, where $b \equiv |\boldsymbol{b}|$). Our factorization theorem has four functions in the IR, the collinear, the global soft, the collinear-soft, the soft-collinear functions, see eq. (2.10)–(2.11), and all of them can potentially contribute to non-perturbative power corrections. Even though the collinear and collinear-soft functions do not contribute to $\boldsymbol{q}_T$ perturbatively, they can still give a non-perturbative power correction to the $\boldsymbol{q}_T$ spectrum.[4]

There are two types of non-perturbative corrections that we will consider here. We call *shift* non-perturbative effects the ones which are not altered by the pass and fail procedure of the grooming conditions. An example is the global soft function that is independent of the grooming procedure and it is common to other TMD analysis. We refer to this kind of correction as *shift* non-perturbative effects since, as we will see later, in the simplest case it generates a shift in the TMD spectrum. The second correction instead is related to the grooming procedure with *cs* and *sc* soft functions and the jet shape function. In this case non-perturbative effects are driven by the so called "non-perturbative particles" and it is obviously only possible when perturbative modes are on the boundary of passing and failing soft-drop. We refer to these contributions as *boundary* non-perturbative effects.

4.1 *Shift* non-perturbative correction

For the case of shift correction, we assume that the soft-drop condition remains unaltered by any non-perturbative emissions. Now consider the contribution to the shift correction by each function in turn.

The non-perturbative part of the global soft function defined in eq. (2.7) has been studied in the literature in several frameworks [30, 46–50]. Up to $\mathcal{O}(b^4)$ terms it can be written as

$$\langle 0|T[S_n S_{\bar{n}}^\dagger(\boldsymbol{b})]\bar{T}[S_{\bar{n}} S_n^\dagger(0)]|0\rangle = \tilde{S}(b) + b^2\,\bar{C}_i^{(s)}(b)\langle 0|O^i|0\rangle\,, \tag{4.1}$$

where O^i is the complete set of local operators that have the same quantum numbers as the soft function. Summation over i is implied. Here $\tilde{S}$ is the perturbative calculable part of the soft function and it contains rapidity and UV divergences as well as the rest of other

---

[4]There are also power corrections of similar magnitude in this region due to the factorization of the *sc* function from the *cs*, but they are perturbative in nature and can be handled by making a smooth transition to region III.

terms in the equation. We can pull this out as a common factor to write

$$\langle 0|T[S_n S_{\bar{n}}^{\dagger}(\boldsymbol{b})]\bar{T}[S_{\bar{n}} S_n^{\dagger}(0)]|0\rangle = \tilde{S}(b)\Big(1 + b^2\, C_i^{(s)}(b)\langle 0|O^i|0\rangle\Big). \tag{4.2}$$

To maintain the UV scale invariance of the cross section, we need that the second term in the brackets be independent of UV divergences. However additional rapidity divergences may be present in the non-perturbative matrix element on the r.h.s. that cancel with the corresponding rapidity divergence arising in the non-perturbative power corrections to the collinear or soft-collinear functions. This is related to the origin of the non-perturbative correction to the rapidity anomalous dimension and it is usually included also in TMD analysis.

We can perform a similar analysis for the soft-collinear (sc) function. When an sc (perturbative) mode passes soft-drop, then it does not contribute to q_T since it becomes part of the groomed jet. But since it has a large $+$ component, it drives the groomed jet mass outside the region of measurement and hence such events are dropped. Therefore, we only need to consider the case when the sc mode fails soft drop. In this case the non-perturbative emission contributes to the q_T measurement if it lies outside the groomed jet. Given the angular scaling of this mode, which is much larger than the collinear-soft (cs) and collinear modes that form the groomed jet, the phase space region available is effectively unconstrained (this is also the reason why we ignore any phase space constraints on the soft non-perturbative emissions). Hence the correction in this case will also be a simple shift type and is implemented in the same manner as in the case of the global soft function. As before, we can pull out a common perturbative factor (that includes the perturbative soft drop condition), and write

$$\tilde{S}_{sc}^{\perp}(b, z_{\text{cut}})|_{\text{hadr.}} = \tilde{S}_{sc}^{\perp}(b, Q z_{\text{cut}})\Big(1 + b^2 C_i^{(sc)}(b, z_{\text{cut}})\,\langle 0|O^i|0\rangle\Big). \tag{4.3}$$

Notice that now all the z_{cut} dependence of the power correction is included in the perturbative calculable coefficient $C^{(sc)}(b, z_{\text{cut}})$, which multiplies the same non-perturbative power correction present also in the global soft function case. The calculation of $C^{(s)}$, $C^{(sc)}$ is doable perturbatively, although this consideration goes beyond the present work.

We can then combine all shift corrections that have an unconstrained phase space for non-perturbative emissions together so that in b space we have a multiplicative correction to the perturbative cross section of the form

$$SS_{sc}^{\perp}|_{\text{hadr.}} = (1 + b^2(\Omega_s + \Omega_{sc}))SS_{sc}^{\perp}|_{\text{pert.}}, \tag{4.4}$$

where Ω_s is the same as the TMD case and Ω_s is a single parameter to be fitted from e^+e^- experiments. It is clear that, in the event of non-trivial $C^{\{(s), (sc)\}}$, $\Omega_{s, sc}$ can have a mild (logarithmic) dependence on q_T so that this model will work well over a limited range of q_T which may be sufficient for most cases.

We now consider the shift corrections coming from the collinear-soft and the collinear functions. Since these modes determine the region of the groomed jet, we can consider two possible scenarios which give a non-trivial power correction.

1. Collinear-soft (cs) particles pass soft-drop:
   If the cs particles pass the soft-drop (for phase space see figure 9(a)) then any non-perturbative emission scaling as the cs mode can contribute to q_T when it lies outside
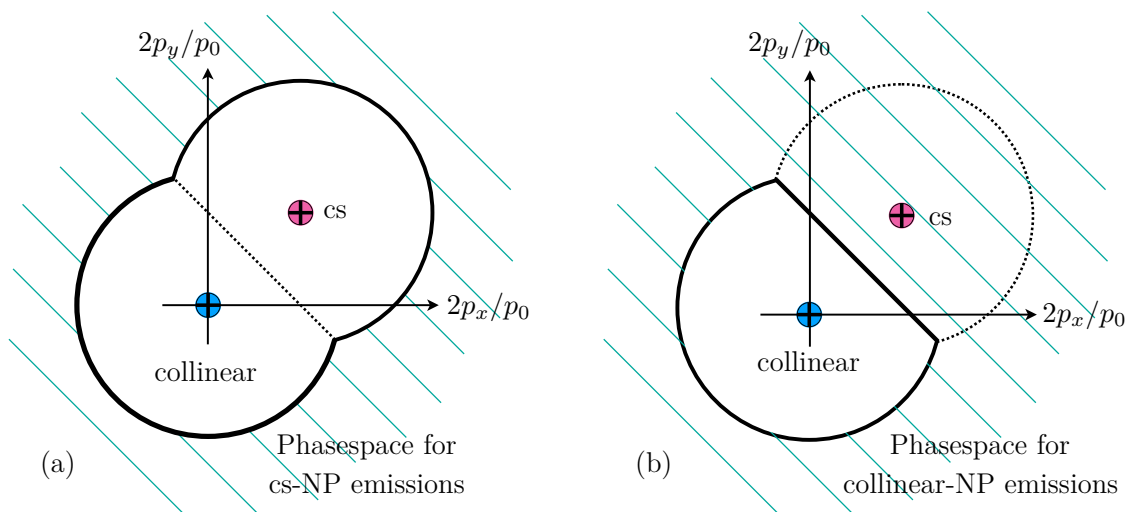
Figure 9. (a) When the collinear-soft (cs) function passes soft drop, the non-perturbative (NP) emissions, with the angular scaling of the cs mode, with a virtuality Λ_{QCD} must fall in the phase space shown by the blue shaded area in order to contribute to q_T. (b) When the cs function fails soft drop, the NP emission with the angular scaling of the collinear modes must not be clustered with the collinear sub-jet in order to contribute to q_T.

the groomed jet. In this case, we need to calculate the catchment area of the groomed jet that is determined by the angular distance of the cs subject that passed soft-drop. As was pointed out in [12], it is possible at NLL, using a coherent branching formalism, to factorize a purely non-perturbative function from all the calculable perturbative effects (including grooming). A detailed analysis of these corrections will be presented in a future work.

2. Collinear-soft particles fail soft-drop:

   In this case collinear modes are the only ones that pass soft-drop (for phase space see figure 9(b)), so that any non-perturbative mode scaling as cs has an unconstrained phase space, by the same logic as for the soft and the sc functions, so that we get a simple shift correction of the same form as the soft, sc and TMD collinear functions.[5] There is another possible interesting correction that will come from the collinear NP emission that lies outside the catchment region that is now determined by the collinear modes alone.

   In this case there are two ways of approaching the problem. In one, we consider separating out the non-perturbative corrections before factorizing the cs and collinear modes. The other way is to realize that in the case where cs fails soft-drop, the entire groomed jet mass measurement comes from the jet function alone and using this condition we can define a catchment area for the collinear non-perturbative emissions *without explicitly accessing any information from the cs function*, so that

---

[5]Technically in this case the perturbative value of $p_{\perp cs}$ would give a larger correction. However, this correction can eventually be handled by transitioning to a new EFT in which the sc and cs functions merge together. For now we will ignore them and only keep track of the other non-perturbative corrections.

the factorization between the collinear and *cs* modes is maintained. In this case, we can do a diagrammatic analysis, similar to [12], for the collinear function, to check if it is possible to factorize the non-perturbative effects from the perturbative. We leave this work for the future.

4.2 Boundary corrections

We now consider boundary corrections that leave the q_T measurement function unchanged but only require an expansion of the soft-drop condition in q^-/Q. The functions that do not explicitly have a soft-drop condition can then be ignored, which leaves us with only the *sc* and *cs* functions. We can follow the same line of reasoning as in [12].

1. *sc* emissions
   In this case we demand that either an addition or removal of the non-perturbative emission cause the soft-collinear function to fail soft-drop. Otherwise it will drive up the jet mass outside the measured range. If we consider a non-perturbative emission q^μ along with a perturbative momentum p^μ, then we can expand out the soft-drop condition in the non-perturbative momentum. We can write the complete measurement function as

$$\Theta^{p\pm q} = \Theta\left(\frac{p+q}{E_J} - z_{\text{cut}}\right)\delta^2(\boldsymbol{p}_{\perp sc} - \boldsymbol{p}_\perp \mp \boldsymbol{q}_T)\,, \qquad (4.5)$$

   where p is the momentum of the perturbative *sc* sub-jet while q^μ is the momentum of the non-perturbative emission. The $\pm$ signs indicate whether the perturbative *cs* subject gains or loses a non-perturbative momentum after hadronization. In the case where the *sc* sub-jet gains a non-perturbative emission, the measurement expanded to leading order looks like

$$\Theta^{p+q} \approx \Theta^p_{sd}\delta^2(\boldsymbol{p}_{\perp sc} - \boldsymbol{p}_\perp) + \frac{q^-}{E_J}\Theta^{\text{b.c.}}(\theta_q, \theta_p, \Delta\phi)\delta^p_{sd}\Big[\delta^2(\boldsymbol{p}_{\perp sc} - \boldsymbol{p}_\perp)\Big]\,, \qquad (4.6)$$
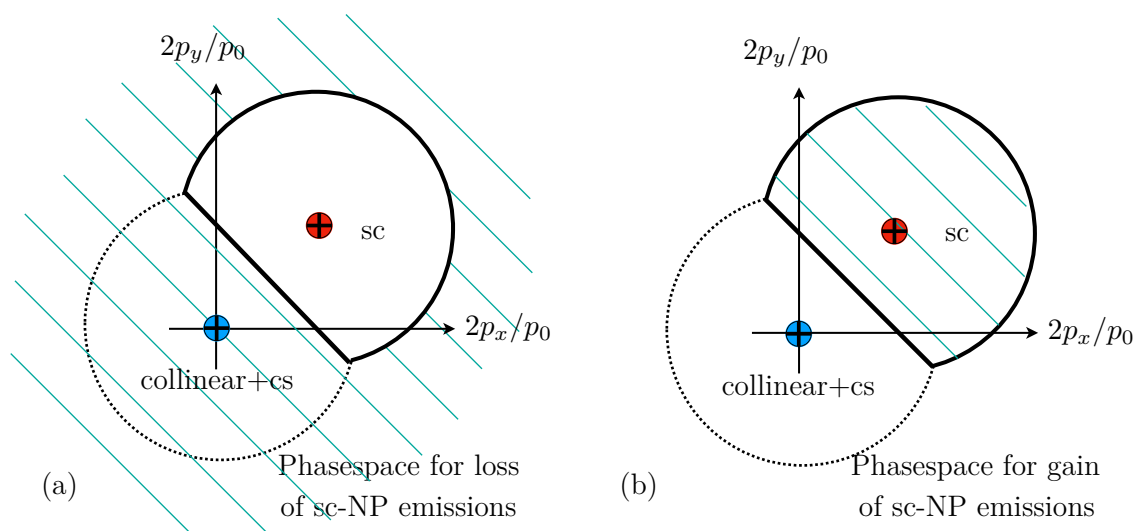
   with

$$\Theta^p_{sd} \equiv \Theta\left(\frac{p}{E_J} - z_{\text{cut}}\right)\,, \qquad\qquad \delta^p_{sd} \equiv \delta\left(\frac{p}{E_J} - z_{\text{cut}}\right)\,. \qquad (4.7)$$

   In this case, the non-perturbative emission q^μ gets clustered with the *sc* subject. Note that we have expanded q_i from the $\boldsymbol{p}_\perp$ measurement since we are working at leading order. The phase-space constraint, $\Theta^{\text{b.c.}}$ (see figure 10(a)), gives the condition that ensures q^μ gets clustered with the *sc* part.

   The second case is when q^μ is emitted off p^μ but it is not clustered with the *sc* jet. The short distance condition now acts on $p - q$, which can then be expanded out to give

$$\Theta^{p-q} \approx \Theta^p_{sd}\delta^2(\boldsymbol{p}_{\perp sc} - \boldsymbol{p}_\perp) - \frac{q^-}{E_J}\bar\Theta^{\text{b.c.}}(\theta_q, \theta_p, \Delta\phi)\delta^p_{sd}\Big[\delta^2(\boldsymbol{p}_{\perp sc} - \boldsymbol{p}_\perp)\Big]\,, \qquad (4.8)$$

Figure 10. (a) The case where the sc subjet loses an NP emission (b) The case when the sc subjet gains an NP emission.

$\bar{\Theta}^{\text{b.c.}}$ (see figure 10(b)) is the phase space region for q^μ so that it falls outside the sc subjet. We can see that the leading power correction scales as q^-/E_J, which, given the angular scaling of the *sc* mode, scales as $q_T z_{\text{cut}}/Q$. Given a typical value of $z_{\text{cut}} \sim 0.1$, this factor is then comparable to the q_T^2/Q^2 correction that we get from the shift terms.

2. Soft-Collinear function

   We expect that since perturbatively this function does not contribute to q_T, the boundary correction should have no effect on the q_T measurement.

We now have listed out all the possible NP corrections to the transverse momentum measurement.

5 Conclusions

In this paper, we have presented the computation of the transverse momentum de-correlation observable for fat jets groomed using the Soft-Drop algorithm. We consider two scattering experiments: $e^+e^- \to$ di-jets and semi-inclusive DIS. In the former, we measure the transverse momentum imbalance between the two groomed jets. We impose a jet mass constraint on our jets in order to ensure collimated jet configurations. Simulation using PYTHIA show that grooming greatly reduces the impact of underlying events as well as final state hadronization. We show that the factorization theorem for this observable involves the universal soft function which also appears in the traditional definition of TMDs. We propose that this observable can be used as a probe of the non-perturbative rapidity anomalous dimension, which is a universal parameter for TMD distributions. We prove within our EFT that the cumulant jet mass constraint only adds to the overall normalization of the perturbative cross section and hence does not impact the shape of the transverse

momentum distribution although it does contribute to the uncertainty. We gather or compute all the ingredients necessary to evaluate the cross section to NNLL accuracy and a numerical study for the cases of interest. In the implementation we have used the `artemide` code [45, 51–53] which contains the most recent extraction TMDPDF at higher perturbative orders. As part of the numerical analysis we have used the ζ-prescription [33] which allows a complete disentanglement of non-perturbative effects of rapidity evolution from the rest. An uncertainty analysis gives us an error band of approximately $\pm$ 10 %. The main ingredient of this error is the perturbative uncertainty which can be systematically improved. As shown in figure 1 the hadronization corrections at low q_T are significantly smaller than the case of a standard jet axis and it is therefore one of the major advantage of using grooming. These effects are expected to be the same in e^+e^- and SIDIS because of the factorization of the cross section. In the case of e^+e^- these corrections constitute all of non-perturbative effects and they are associated with the final state shower. In order to do a meaningful extraction of non-perturbative parameters in this case, it is therefore necessary to improve the uncertainty from perturbative physics to be better than 5%. This can be achieved by moving to a higher order in resummation accuracy (N3LL). This is something we leave as a follow up to this paper.

In the SIDIS case we measure the transverse momentum imbalance between the groomed jet and the recoiling lepton. Once again we demand a jet mass measurement in order to ensure sensitivity to collinear physics only. A large part of the contribution to this comes from the soft and collinear radiation that lies outside the jet and, for low transverse momentum, probes the complete TMDPDF. The cross section is again presented to NNLL accuracy and involve much of the same ingredients as in the case of $e^+e^- \to$ dijets. A higher order perturbative calculation is expected to reduce significatevely errors also in this case.

Concerning the hadronization effects we observe that grooming the jet allows us to have a wide angle jet, which is preferred in low energy experiments, while still being free from non-global logarithms, which are non-factorizable and they are usually present in ungroomed jets. Nevertheless it is possible to measure directly the hadronization effects due to grooming. The idea is to parametrize and extract all of the non-perturbative effects from $e^+e^- \to$ dijets and use them in SIDIS since they contain all the same matrix elements (in addition to the TMDPDF) as explained in section 4. This gives us a robust way to access the TMDPDF while maintaining control over all other uninteresting non-perturbative effects.

Acknowledgments

A   Laplace and Fourier transformations

We define the Fourier transform, $\mathcal{FT}[f](\boldsymbol{b}) = f(\boldsymbol{b})$ of a function, $f(\boldsymbol{q}_T) = \mathcal{FT}^{-1}[f](\boldsymbol{q}_T)$ as follows,

$$f(\boldsymbol{b}) = \int_{-\infty}^{+\infty} d\boldsymbol{q}_T \ f(\boldsymbol{q}_T) \exp(-i\boldsymbol{b} \cdot \boldsymbol{q}_T) , \qquad (A.1)$$

and the inverse transform

$$f(\boldsymbol{q}_T) = \int_{-\infty}^{+\infty} \frac{d\boldsymbol{b}}{(2\pi)^2} f(\boldsymbol{b}) \exp(i\boldsymbol{b} \cdot \boldsymbol{q}_T) . \qquad (A.2)$$

In order to get the Fourier transforms of the plus distributions that appear in the factorization theorem we use,

$$\frac{1}{(2\pi)\,\mu^2} \left(\frac{\mu^2}{q_T^2} \right)^{1+\alpha} = -\frac{1}{2\alpha} \delta^{(2)}(\boldsymbol{q}_T) + \mathcal{L}_0(q_T^2, \mu^2) - \alpha\mathcal{L}_1(q_T^2, \mu^2) + \mathcal{O}(\alpha^2) . \qquad (A.3)$$

Taking the Fourier transform of the left-hand-side (l.h.s.) we get (see eq. (E.2) of ref. [26])

$$\int_{-\infty}^{+\infty} \frac{d\boldsymbol{q}_T}{(2\pi)} \frac{1}{\mu^2} \left(\frac{\mu^2}{q_T^2} \right)^{1+\alpha} \exp(-i\boldsymbol{b} \cdot \boldsymbol{q}_T) = -\frac{e^{-2\alpha\gamma_E}}{2\alpha} \frac{\Gamma(1-\alpha)}{\Gamma(1+\alpha)} \left(\frac{\mu}{\mu_E} \right)^{2\alpha}$$

$$= -\frac{1}{2\alpha} + \ln\left(\frac{\mu}{\mu_E} \right) + \alpha\ln^2\left(\frac{\mu}{\mu_E} \right) + \mathcal{O}(\alpha^2) , \qquad (A.4)$$

where $\mu_E = 2\exp(-\gamma_E)/b$ and $b \equiv |\boldsymbol{b}|$ and in the second line we expanded in α. Comparing this result with the r.h.s. of eq. (A.3) we get,

$$\mathcal{FT}\Big[\delta^{(2)}(\boldsymbol{q}_T)\Big](\boldsymbol{b}) = 1 ,$$

$$\mathcal{FT}\Big[\mathcal{L}_0(q_T^2, \mu^2)\Big](\boldsymbol{b}) = \ln\left(\frac{\mu_E}{\mu} \right) ,$$

$$\mathcal{FT}\Big[\mathcal{L}_1(q_T^2, \mu^2)\Big](\boldsymbol{b}) = \ln^2\left(\frac{\mu_E}{\mu} \right) . \qquad (A.5)$$

We define the convolution $f \otimes g$ with

$$\Big[f \otimes g\Big](\boldsymbol{q}_T) = \int d\boldsymbol{\ell}_\perp \ f(\boldsymbol{q}_T - \boldsymbol{\ell}_\perp) g(\boldsymbol{\ell}_\perp) , \qquad (A.6)$$

such that

$$\mathcal{F}\Big[f \otimes g\Big](\boldsymbol{b}) = f(\boldsymbol{b}) \times g(\boldsymbol{b}) . \qquad (A.7)$$

Similarly for the distribution in the jet-thrust we often work in Laplace space where the corresponding convolutions translate to products. For these reason we define the Laplace transformation $\mathcal{LT}[f](s) = f(s)$ of jet-trust distribution $f(e) = \mathcal{LT}^{-1}[f](e)$ as follows:

$$f(s) = \int_{-\infty}^{\infty} de \, \exp(-se)f(e)\,, \tag{A.8}$$

and the corresponding inverse transform

$$f(e) = \frac{1}{2\pi i} \int_{\gamma-i\infty}^{\gamma+i\infty} ds \, \exp(se)f(s)\,. \tag{A.9}$$

Similarly with the case of Fourier transform we use the following expansion to identify the Laplace transform of plus distributions that are present in the fixed order expansion of the jet and collinear-soft functions,

$$\frac{1}{\xi}\left(\frac{\xi}{e}\right)^{1+\alpha}|_{e>0} = -\frac{1}{\alpha}\delta(e) + \mathcal{L}_0(e,\xi) - \alpha\mathcal{L}_1(e,\xi) + \mathcal{O}(\alpha^2)\,, \tag{A.10}$$

taking the Laplace transform of the l.h.s. we get

$$\int_0^\infty \frac{de}{\xi}\left(\frac{\xi}{e}\right)^{1+\alpha}\exp(-se) = s^\alpha \Gamma(-\alpha) = -\frac{1}{\alpha} - \ln(\xi\tilde{s}) - \alpha\left(\frac{1}{2}\ln^2(\xi\tilde{s}) + \frac{\pi^2}{12}\right) + \mathcal{O}(\alpha^2)\,, \tag{A.11}$$

where $\tilde{s} \equiv s\exp(\gamma_E)$ and thus from comparing eq. (A.10) and (A.11) we have

$$\mathcal{LT}\Big[\delta(e)\Big](s) = 1\,,$$
$$\mathcal{LT}\Big[\mathcal{L}_0(e,\xi)\Big](s) = -\ln(\xi\tilde{s})\,,$$
$$\mathcal{LT}\Big[\mathcal{L}_1(e,\xi)\Big](s) = \frac{1}{2}\ln^2(\xi\tilde{s}) + \frac{\pi^2}{12}\,. \tag{A.12}$$

B Operator definitions and one loop results

In this appendix we give the operator definitions of the factorization elements and their NLO expansions. From those we determine the renormalization functions, group equations, and corresponding anomalous dimensions. Many of the results presented here are already known and found in literature.

B.1 Jet functions

The quark and gluon jet function definitions, one loop calculation, and the corresponding Laplace transforms can be found in ref. [43]. Here we summarize their results. The quark jet function is given by,

$$J_q(e, Q) = \frac{(2\pi)^3}{N_c}\text{tr} \, \langle \frac{\bar{\slashed{n}}}{2}\chi_n(0)\delta(Q - \mathcal{P}^-)\delta^{(2)}(\boldsymbol{\mathcal{P}}_\perp)\delta(e - \mathcal{E})\bar{\chi}_n \rangle\,, \tag{B.1}$$

and the gluon

$$J_q(e, Q) = \frac{(2\pi)^3}{N_c}\text{tr} \, \langle \frac{\bar{\slashed{n}}}{2}\mathcal{B}_{n\perp}^\mu(0)\delta(Q - \mathcal{P}^-)\delta^{(2)}(\boldsymbol{\mathcal{P}}_\perp)\delta(e - \mathcal{E})\mathcal{B}_{n\perp\mu} \rangle\,, \tag{B.2}$$

where N_c is the number of colors and $\mathcal{B}_{n\perp}^\mu$ is the gauge invariant gluon building block of the effective field theory,

$$\mathcal{B}_{n\perp}^\mu = \frac{1}{g}[W_n^\dagger(\mathcal{P}_\perp^\mu + gA_{n,\perp}^\mu)W_n].\tag{B.3}$$

As demonstrated earlier when working with the cumulant distribution (i.e., when integrating out to $e_{\rm cut}$) it is useful to work in Laplace space. The renormalized groomed jet function up to NLO contributions in Laplace space is given by

$$J_i(s,Q;\mu) = 1 + \frac{\alpha_s C_i}{2\pi}\left\{L_J^2 + \bar{\gamma}_i L_J - \frac{\pi^2}{3} + c_i\right\} + \mathcal{O}(\alpha_s^2),\tag{B.4}$$

where for quark initiated jets we have

$$C_q = C_F = \frac{N_c^2 - 1}{2N_c}, \qquad \bar{\gamma}_q = \frac{3}{2}, \qquad c_q = \frac{7}{2},\tag{B.5}$$

and for gluon initiated jets we have

$$C_g = C_A = N_c, \qquad \bar{\gamma}_g = \frac{\beta_0}{2C_A}, \qquad c_g = \frac{67}{18} - \frac{10}{9}\frac{n_f T_R}{C_A}.\tag{B.6}$$

The logarithms, L_J that appear in eq. (B.4) and the corresponding one loop anomalous dimensions are

$$L_J = \ln\left(\frac{\mu^2 \tilde{s}}{Q^2}\right), \qquad \gamma^J = \frac{\alpha_s C_i}{\pi}\left(2L_J + \bar{\gamma}_i\right) + \mathcal{O}(\alpha_s^2).\tag{B.7}$$

The anomalous dimension is defined through the RG equation satisfied by renormalized jet functions. In Laplace space this is

$$\frac{d}{d\ln\mu}J_i(s,Q;\mu) = \gamma^J(s,Q;\mu)J_i(s,Q;\mu).\tag{B.8}$$

In momentum space the above equation is written as convolution (in the invariant mass variable e), of the anomalous dimension and the renormalized jet function.

B.2 Collinear-soft function

The operator definition of the invariant mass measurement collinear soft function is given by

$$S_{cs}(e,Qz_{\rm cut}) = \frac{1}{N_R}{\rm tr}\langle T\left(U_n^\dagger W_t\right)\mathcal{M}_e^{\rm SD}\bar{T}\left(W_t^\dagger U_n\right)\rangle,\tag{B.9}$$

where $\mathcal{M}_e^{\rm SD}$ is the invariant measurement function,

$$\mathcal{M}_e^{\rm SD} = \delta\left(e - (1 - \Theta_{\rm SD})\,\mathcal{E}\right).\tag{B.10}$$

Here we dropped the jet flavor (quark/anti-quark or gluon) for simplicity of notation and the normalization constant N_R is simply the size of the representation for SU(N_c) of the W_t and U_n Wilson lines. For quark jets (fundamental representation) we have $N_R = N_c$ and

for gluon jets (adjoint representation) we have $N_R = N_c^2 - 1$. At NLO the bare collinear soft function is given by

$$S_{cs,\text{bare}}(e, Qz_{\text{cut}}) = \delta(e) + \frac{\alpha_s C_i}{\pi} \left\{ -\frac{1}{\epsilon^2}\delta(e) + \frac{1}{\epsilon}\mathcal{L}_0(e, \xi) - \mathcal{L}_1(e, \xi) + \frac{\pi^2}{12}\delta(e) \right\} + \mathcal{O}(\alpha_s^2),$$

(B.11)

where

$$\xi \equiv \frac{\mu^2}{Q^2 z_{\text{cut}}}.$$

(B.12)

Therefore we have for the renormalized function

$$S_{cs}(e, Qz_{\text{cut}}) = \delta(e) + \frac{\alpha_s C_i}{\pi} \left\{ -\mathcal{L}_1(e, \xi) + \frac{\pi^2}{12}\delta(e) \right\} + \mathcal{O}(\alpha_s^2),$$

(B.13)

where

$$S_{cs,\text{bare}}(e, Qz_{\text{cut}}) = Z_{cs} \otimes S_{cs}(e, Qz_{\text{cut}}),$$

(B.14)

with

$$Z_{cs}(e) = \delta(e) + \frac{\alpha_s C_i}{\pi} \left\{ -\frac{1}{\epsilon^2}\delta(e) + \frac{1}{\epsilon}\mathcal{L}_0(e, \xi) \right\} + \mathcal{O}(\alpha_s^2).$$

(B.15)

In Laplace space for the renormalized collinear-soft function we get,

$$S_{cs}(s, Qz_{\text{cut}}; \mu) = 1 - \frac{\alpha_s C_i}{2\pi} L_{cs}^2 + \mathcal{O}(\alpha_s^2),$$

(B.16)

which satisfies the following RGE

$$\frac{d}{d\ln\mu} S_{cs}(s, Qz_{\text{cut}}; \mu) = \gamma^{cs}(s, \mu) S_{cs}(s, Qz_{\text{cut}}; \mu).$$

(B.17)

The logarithm L_{cs} and the corresponding anomalous dimension are

$$L_{cs} = \ln(\xi\tilde{s}), \qquad\qquad \gamma^{cs}(s, \mu) = -2\frac{\alpha_s C_i}{\pi} L_{cs} + \mathcal{O}(\alpha_s^2).$$

(B.18)

B.3 Soft function

The soft function that appears in the factorization theorems in eq. (2.15) and (3.4) is defined in eq. (2.7) and it has been calculated in several schemes at higher orders in QCD, as reported in section 2.2. Here we report a one loop expression using the analytic regulator in momentum space,

$$S_{\text{bare}} = \delta^{(2)}(\boldsymbol{q}_T) + \frac{\alpha_s(\mu) C_i}{\pi} \left\{ \frac{4}{\eta} \left[\mathcal{L}_0(q_T^2, \mu^2) - \frac{1}{2\epsilon}\delta^{(2)}(\boldsymbol{q}_T) \right] + \frac{1}{\epsilon} \left[\frac{1}{\epsilon} - 2\ln\left(\frac{\nu}{\mu}\right) \right] \delta^{(2)}(\boldsymbol{q}_T) \right.$$
$$\left. + 4\mathcal{L}_0(q_T^2, \mu^2)\ln\left(\frac{\nu}{\mu}\right) - 2\mathcal{L}_1(q_T^2, \mu^2) - \frac{\pi^2}{12}\delta^{(2)}(\boldsymbol{q}_T) \right\} + \mathcal{O}(\alpha_s^2).$$

(B.19)

The renormalized soft function, S, is defined through

$$S_{\text{bare}} = Z_s^\perp(\mu, \nu) \otimes S(\mu, \nu),$$

(B.20)

(a) virtual gluon   (b) real gluon
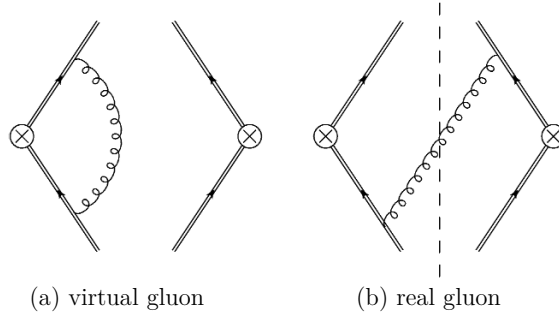
Figure 11. The order $\mathcal{O}(\alpha_s)$ diagrams that contribute to the soft-collinear function.

and satisfies the following renormalization group equations

$$\frac{d}{d\ln\mu}S(\mu,\nu) = \gamma^s(\mu,\nu)S(\mu,\nu)\,, \qquad \frac{d}{d\ln\nu}S(\mu,\nu) = \gamma_\nu^s(\mu,\nu) \otimes S(\mu,\nu)\,. \qquad (B.21)$$

Therefore we find for the one-loop corresponding impact parameter space quantities

$$S(\mu,\nu) = 1 + \frac{\alpha_s(\mu)\,C_i}{\pi}\left\{4\ln\left(\frac{\mu_E}{\mu}\right)\ln\left(\frac{\nu}{\mu}\right) - 2\ln^2\left(\frac{\mu_E}{\mu}\right) - \frac{\pi^2}{12}\right\} + \mathcal{O}\left(\alpha_s^2\right)\,, \quad (B.22)$$

$$Z_s^\perp(\mu,\nu) = 1 + \frac{\alpha_s(\mu)\,C_i}{\pi}\left\{\frac{4}{\eta}\left[\ln\left(\frac{\mu_E}{\mu}\right) - \frac{1}{2\epsilon}\right] + \frac{1}{\epsilon}\left[\frac{1}{\epsilon} - 2\ln\left(\frac{\nu}{\mu}\right)\right]\right\} + \mathcal{O}(\alpha_s^2)\,, \quad (B.23)$$

with

$$\gamma^s(\mu,\nu) = -4\frac{\alpha_s(\mu)\,C_i}{\pi}\ln\left(\frac{\nu}{\mu}\right) + \mathcal{O}\left(\alpha_s^2\right)\,, \quad \gamma_\nu^s(\mu,\nu) = 4\frac{\alpha_s(\mu)\,C_i}{\pi}\ln\left(\frac{\mu_E}{\mu}\right) + \mathcal{O}(\alpha_s^2)\,. \tag{B.24}$$

The rapidity and renormalization scales used to produce our result are fixed using the ζ-prescription [33] adapted for this case. Later in the appendix we give a description of how one can use the rapidity regulated objects that have ν dependence to construct the subtracted rapidity divergences free objects but yet keep trace of the rapidity logs using the ζ parameter.

B.4   Soft-collinear function

The soft-collinear function is defined by the matrix element

$$S_{sc}^\perp(Qz_{\text{cut}}) = \frac{1}{N_R}\text{tr}\langle T\left(U_n^\dagger W_t\right)\mathcal{M}_\perp^{\text{SD}}\bar{T}\left(W_t^\dagger U_n\right)\rangle\,, \tag{B.25}$$

and the groomed jet measurement function, $\mathcal{M}_\perp^{\text{SD}}$ is given in terms of the label momentum operator, $\mathcal{P}$,

$$\mathcal{M}_\perp^{\text{SD}} = \Theta_{\text{SD}} \times \delta^2\left(\boldsymbol{q}_T - \Theta_{\text{SD}}\boldsymbol{\mathcal{P}}_\perp\right)\,, \tag{B.26}$$

where Θ_{SD} denotes the soft drop groomer. The collinear-soft modes only contribute to the invariant mass measurement if they pass soft-drop, which is implemented by the Θ_{SD} term. The NLO calculation involves one real and one virtual diagram shown in figure 11. While

the virtual diagram is scaleless. The diagram with a real gluon needs to be integrated over the phase-space of soft gluon. This then yields non-vanishing contribution from when the soft gluon fails the grooming,

$$
S_{sc,\text{NLO}}^{\perp}(Qz_{\text{cut}}) = 4g^2 C_i \tilde{\mu}^{2\epsilon} \, \nu^{\eta} \int \frac{d^d k}{(2\pi)^{d-1}} \frac{\delta(k^2)\,\delta^{(2)}(\boldsymbol{q}_T - \boldsymbol{k}_{\perp})}{k^+ \, (k^-)^{1+\eta}} \theta(Qz_{\text{cut}} - k^-) \,. \tag{B.27}
$$

Performing the integrals we find for the bare quantity

$$
S_{sc,\text{bare}}^{\perp}(Qz_{\text{cut}}) = \delta^{(2)}(\boldsymbol{q}_T) + \frac{\alpha_s C_i}{\pi} \left\{ -\frac{2}{\eta} \Big[\mathcal{L}_0(q_T^2, \mu^2) - \frac{1}{2\epsilon} \delta^{(2)}(\boldsymbol{q}_T) \Big] + \frac{1}{\epsilon} \ln\left(\frac{\nu}{Qz_{\text{cut}}}\right) \delta^{(2)}(\boldsymbol{q}_T) \right.
$$
$$
\left. -2 \ln\left(\frac{\nu}{Qz_{\text{cut}}}\right) \mathcal{L}_0(q_T^2, \mu^2) \right\} + \mathcal{O}(\alpha_s^2) \,, \tag{B.28}
$$

and for the renormalized quantity, $S_{sc,}^{\perp}(Qz_{\text{cut}}; \mu, \nu)$ we have

$$
S_{sc,\text{bare}}^{\perp}(Qz_{\text{cut}}) = Z_{sc}^{\perp}(\mu, \nu) \otimes S_{sc}^{\perp}(Qz_{\text{cut}}; \mu, \nu) \,, \tag{B.29}
$$

and satisfies the following renormalization group equations

$$
\frac{d}{d \ln \nu} S_{sc}^{\perp}(\mu, \nu) = \gamma_{\nu}^{sc}(\mu, \nu) \otimes S_{sc}^{\perp}(\mu, \nu) \,, \qquad \frac{d}{d \ln \mu} S_{sc}^{\perp}(\mu, \nu) = \gamma^{sc}(\mu, \nu) S_{sc}^{\perp}(\mu, \nu) \,, \tag{B.30}
$$

where the Qz_{cut} dependence is suppressed to improve readability. In $\overline{\text{MS}}$ scheme the corresponding Fourier transform can be obtained using eq. (A.5):

$$
\tilde{S}_{sc}^{\perp}(Qz_{\text{cut}}; \mu, \nu) = 1 + \frac{\alpha_s C_i}{\pi} \left\{ -2 \ln\left(\frac{\nu}{Qz_{\text{cut}}}\right) \ln\left(\frac{\mu_E}{\mu}\right) \right\} + \mathcal{O}\left(\alpha_s^2\right) \,, \tag{B.31}
$$

$$
\tilde{Z}_{sc}^{\perp}(\mu, \nu) = 1 + \frac{\alpha_s C_i}{\pi} \left\{ -\frac{2}{\eta} \left[\ln\left(\frac{\mu_E}{\mu}\right) - \frac{1}{2\epsilon} \right] + \frac{1}{\epsilon} \ln\left(\frac{\nu}{Qz_{\text{cut}}}\right) \right\} + \mathcal{O}\left(\alpha_s^2\right) \,, \tag{B.32}
$$

and thus for the one-one-loop anomalous dimensions we get

$$
\begin{aligned}
\gamma_{\nu}^{sc}(\mu, \nu) &= -2 \frac{\alpha_s(\mu) C_i}{\pi} \ln\left(\frac{\mu_E}{\mu}\right) + \mathcal{O}\left(\alpha_s^2\right) \\
\gamma^{sc}(\mu, \nu) &= 2 \frac{\alpha_s(\mu) C_F}{\pi} \ln\left(\frac{\nu}{Qz_{\text{cut}}}\right) + \mathcal{O}(\alpha_s^2) \,.
\end{aligned} \tag{B.33}
$$

C Solution of renormalization group evolution equations

In this appendix we discuss the solutions of both virtuality and rapidity renormalization group equations written in eq. (2.23). All factorization elements (hard, soft, soft-collinear, collinear-soft, and jet) satisfy renormalization group equations, but only transverse momentum dependent quantities have rapidity RGE.

Function	Γ_0^G	γ_0^G	m_G
H_{ij}	$-4(C_i + C_{\bar{j}})$	$-4\bar{\gamma}_i(C_i + C_j)$	Q
S_{cs}	$-8C_i$	0	$Q\sqrt{z_{\text{cut}}/\tilde{s}}$
J_i	$8C_i$	$4\bar{\gamma}_i C_i$	$Q/\sqrt{\tilde{s}}$
$B_{i/h}$	0	$4\bar{\gamma}_i C_i + \gamma_{sc}^0$	0
S	$4(C_i + C_j)$	0	ν_s
$S_{sc}^{\perp}$	0	γ_0^{sc}	n.a

Table 1. Anomalous dimensions coefficients for up to NLL accuracy: $\bar{\gamma}_q = 3/2$, $\bar{\gamma}_g = \beta_0/(2C_A)$, and $\gamma_0^{sc} = 2\alpha_s(\mu)C_F/\pi \ln(\nu/Qz_{\text{cut}})$.

C.1 Renormalization group evolution

The solution to the RGE in eq. (2.23) is

$$G(\mu) = \mathcal{U}_G(\mu, \mu_0)G(\mu_0), \qquad \mathcal{U}_G(\mu, \mu_0) = \exp\left(K_G(\mu, \mu_0)\right)\left(\frac{\mu_0}{m_G}\right)^{2\,\omega_G(\mu, \mu_0)}, \qquad (\text{C.1})$$

with

$$K_G(\mu, \mu_0) = 2\int_{\alpha(\mu_0)}^{\alpha(\mu)} \frac{d\alpha}{\beta[\alpha]}\Gamma^G[\alpha]\int_{\alpha(\mu_0)}^{\alpha} \frac{d\alpha'}{\beta[\alpha']} + \int_{\alpha(\mu_0)}^{\alpha(\mu)} \frac{d\alpha}{\beta[\alpha]}\Delta\gamma^G[\alpha], \qquad (\text{C.2})$$

$$\omega_G(\mu, \mu_0) = \int_{\alpha(\mu_0)}^{\alpha(\mu)} \frac{d\alpha}{\beta[\alpha]}\Gamma^G[\alpha]. \qquad (\text{C.3})$$

Since in this work we are interested only in the NLL and NLL' result we may keep only the first two terms in the perturbative expansion of the cusp part (i.e., Γ_0^G, Γ_0^{cusp}, and Γ_1^{cusp}) and only the first term form the non-cusp part (γ_0^G). Performing this expansion we get,

$$K_G(\mu, \mu_0) = -\frac{\gamma_0^G}{2\beta_0}\ln r - \frac{2\pi\Gamma_0^G}{(\beta_0)^2}\left[\frac{r-1-r\ln r}{\alpha_s(\mu)} + \left(\frac{\Gamma_1^{\text{cusp}}}{\Gamma_0^{\text{cusp}}} - \frac{\beta_1}{\beta_0}\right)\frac{1-r+\ln r}{4\pi} + \frac{\beta_1}{8\pi\beta_0}\ln^2 r\right], \qquad (\text{C.4})$$

$$\omega_G(\mu, \mu_0) = -\frac{\Gamma_0^G}{2\beta_0}\left[\ln r + \left(\frac{\Gamma_{\text{cusp}}^1}{\Gamma_{\text{cusp}}^0} - \frac{\beta_1}{\beta_0}\right)\frac{\alpha_s(\mu_0)}{4\pi}(r-1)\right], \qquad (\text{C.5})$$

where $r = \alpha(\mu)/\alpha(\mu_0)$ and β_n are the coefficients of the QCD β-function,

$$\beta[\alpha_s] = \mu\frac{d\alpha_s}{d\mu} = -2\alpha_s\sum_{n=0}^{\infty}\left(\frac{\alpha_s}{4\pi}\right)^{1+n}\beta_n. \qquad (\text{C.6})$$

The expressions for all ingredients necessary to perform the evolution of any function that appears in the factorization theorems we considered in this paper are given in table 1. The

coefficients for the expansion of the cusp anomalous dimension are

$$\Gamma_0^{\text{cusp}} = 4C_F \,,$$

$$\Gamma_1^{\text{cusp}} = 4C_F \left[\left(\frac{67}{9} - \frac{\pi^2}{3} \right) C_A - \frac{20}{9} n_f T_R \right] \,,$$

$$\Gamma_2^{\text{cusp}} = 4C_F \left[\left(\frac{245}{6} - \frac{134}{27}\pi^2 + \frac{11}{45}\pi^4 + \frac{22}{3}\zeta_3 \right) C_A^2 + \left(-\frac{209}{108} + \frac{5}{27}\pi^2 - \frac{7}{3}\zeta_3 \right) 8C_A n_f T_R \right.$$
$$\left. + \left(16\zeta_3 - \frac{15}{3}C_F n_f T_R - \frac{64}{27}T_R^2 n_f^2 \right) \right] \,. \tag{C.7}$$

The two loop non-cusp anomalous dimensions we need to NNLL RGEs are given by ref. [43]

$$\frac{1}{2}\gamma_1^s + \gamma_1^{sc} = \frac{C_i}{2}\left[34.01C_F + \left(\frac{1616}{27} - 56\zeta_3 - 9.31 \right) C_A - \left(\frac{448}{27} + 14.04 \right) n_f T_R - \frac{2}{3}\pi^2\beta_0 \right] \,,$$

$$\gamma_1^{cs} = C_i\left[-17.00C_F + \left(-55.20 + \frac{22}{9}\pi^2 + 56\zeta_3 \right) C_A + \left(23.61 - \frac{8}{9}\pi^2 \right) n_f T_R \right]$$

$$\gamma_1^q = C_F\left[(3 - 4\pi^2 + 48\zeta_3) C_F + \left(\frac{1769}{27} + \frac{22}{9}\pi^2 - 80\zeta_3 \right) C_A \right.$$
$$\left. + \left(-\frac{484}{27} - \frac{8}{9}\pi^2 \right) n_f T_R \right] \,,$$

$$\gamma_1^s + \gamma_1^{sc} + \gamma_1^B = C_i\left[(20 - 4\pi^2 + 48\zeta_3) C_F + \left(60.87 + \frac{22}{9}\pi^2 - 80\zeta_3 \right) C_A \right.$$
$$\left. + \left(-24.94 - \frac{8}{9}\pi^2 \right) n_f T_R \right] \,. \tag{C.8}$$

C.2 The connection between ζ-parameter and rapidity regulator

In the standard EFT approach one used the rapidity renormalization group (RRG) equations in order to resum large logarithms at the level of individual rapidity regulated terms [26, 37]. A more recent approach for performing the resummation of large logarithms in the TMD evolution it was introduced in ref. [33]. The approach is referred to as the ζ-prescription. Here we rewrite the fixed order results using the rapidity regulator in the past sections in the form appropriate for implementing the ζ-prescription. In the framework of ref. [33] one works with the rapidity divergent free quantity,

$$S_{sc}^{sub}(b; \mu, \zeta) \equiv \sqrt{S_2^\perp(\boldsymbol{b}; \mu, \nu_s)} \, S_{sc}^\perp(\boldsymbol{b}, Q z_{\text{cut}}; \mu, \nu_{sc}) \,, \tag{C.9}$$

where we have explicitly show the dependence on the rapidity regulator parameters ν_s and ν_{sc}. In the RRG approach this combination does not acquire rapidity evolution thus here in order to establish the rapidity evolution we fix the rapidity scales at two different values. Particularly we evaluate the soft-collinear rapidity scale at its canonical value, $\nu_{sc} = Q z_{\text{cut}}$, and we allow for the corresponding soft scale to float through a parameter ζ: $\nu_s = \sqrt{\zeta}$.[6] With this choice of scales we have,

$$S_{sc}^{sub}(b; \mu, \zeta) = 1 + \frac{\alpha_s(\mu)C_i}{2\pi}\left\{ 2\ln\left(\frac{\mu_E}{\mu} \right)\ln\left(\frac{\zeta}{\mu^2} \right) - 2\ln^2\left(\frac{\mu_E}{\mu} \right) - \frac{\pi^2}{12} \right\} + \mathcal{O}(\alpha_s^2) \,. \tag{C.10}$$

---

[6]Note that this is not a unique choice of scales since any choice for which $\nu_s/\nu_{sc} = \sqrt{\zeta}/(Q z_{\text{cut}})$ will give the same result.

And according to the notation of eq. (2.20) and (2.21) satisfies the following equations

$$\mu^2 \frac{d}{d\mu^2} S_{sc}^{sub}(b;\mu,\zeta) = \frac{1}{2} \gamma^{sc/sub}(\mu,\zeta) S_{sc}^{sub}(b;\mu,\zeta) \,,$$
$$\zeta \frac{d}{d\zeta} S_{sc}^{sub}(b;\mu,\zeta) = -\mathcal{D}(\mu) S_{sc}^{sub}(b;\mu,\zeta) \,. \tag{C.11}$$

Its easy to show that the anomalous dimensions $\gamma^{sc/sub}$ and $\mathcal{D}$ are related to the RG and RRG anomalous dimensions of the global soft and soft-collinear function as follows,

$$\gamma^{sc/sub}(\mu,\zeta) = \frac{1}{2}\gamma^s + \gamma^{sc} = \Gamma^{\rm cusp}[\alpha_s] \ln\left(\frac{\mu^2}{\zeta}\right) + \frac{1}{2}\Delta\gamma^s[\alpha_s] + \Delta\gamma^{sc}[\alpha_s] \,, \tag{C.12}$$

and

$$\mathcal{D}(\mu) = \Gamma^{\rm cusp}[\alpha_s] \ln\left(\frac{\mu}{\mu_E}\right) - \frac{1}{4}\Delta\gamma^s_\nu[\alpha_s] \,, \tag{C.13}$$

where

$$\Delta\gamma^s_\nu = -\left(\frac{\alpha_s(\mu)}{4\pi}\right)^2 C_i \left[\left(\frac{128}{9} - 56\zeta_3\right) C_A + \frac{112}{9}\beta_0\right] + \mathcal{O}(\alpha_s^3). \tag{C.14}$$

It is easy to confirm by looking the above equations that the anomalous dimensions $\gamma^{sc/sub}$ and $\mathcal{D}$ satisfy the following differential equations,

$$\frac{d}{d\ln\zeta}\gamma^{sc/sub}(\mu,\zeta) = -\Gamma_{\rm cusp} \,, \qquad\qquad \frac{d}{d\ln\mu}\mathcal{D}(\mu) = +\Gamma_{\rm cusp} \,. \tag{C.15}$$

Also comparing against the notation of eq. (2.23) we see that the non-cusp part, $\Delta\gamma^{sc/sub}$, of the anomalous dimension $\gamma^{sc/sub}$ is a linear combination of the corresponding non-cusp pieces of the global soft and soft-collinear functions. Particularly:

$$\Delta\gamma^{sc/sub}(\mu) = \left(\frac{1}{2}\Delta\gamma^s[\alpha_s(\mu)] + \Delta\gamma^{sc}[\alpha_s(\mu)]\right) \,, \tag{C.16}$$

and this statement is true to all orders in perturbative expansion.

C.3 ζ-prescription

The implementation of the ζ-prescription leads to the definition of optimal TMDs. We sketch here the procedure to obtain optimal TMDs referring to the original work [33] for further details. The anomalous dimensions $\gamma_F(\mu,\zeta)$ and $\mathcal{D}(\mu,b)$ governing the evolution can be thought as two components of a vector field in the plane $(\ln\mu^2, \ln\zeta)$. The integrability condition, e.g. eq. (C.15), states that such field is irrotational, i.e. locally conservative. This allows to define a scalar potential and guarantees that the evolution between two points in the $(\ln\mu^2, \ln\zeta)$ space is independent of the path; in particular, no evolution occurs along equipotential lines. However, the perturbative expansion breaks the validity of such statement and in fact it was shown that numerical predictions largely depend on the choice of path. This limit is overcome by the *improved γ solution*, that reinstates path-invariance
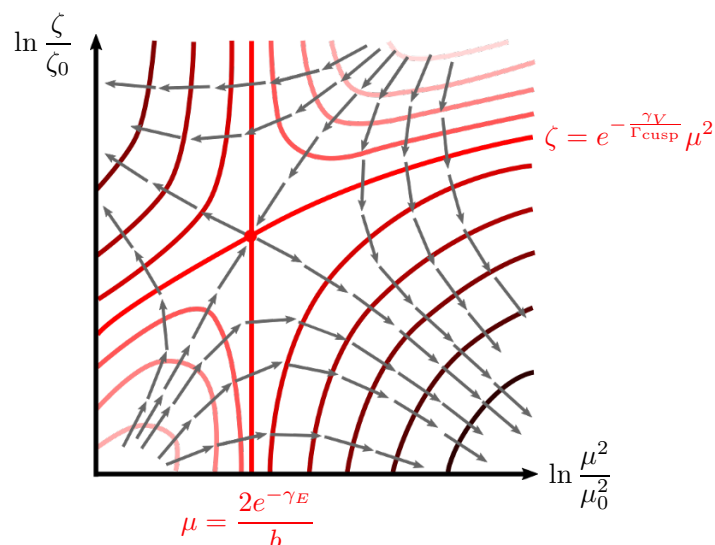
Figure 12. Sketch of the geometry of the (ζ, μ) plane where the double scale evolution takes place. The anomalous dimensions determine a conservative field (grey arrows) and the evolution is null among equipotential lines (shades of red). The intersection of two special equipotential lines (bright red) determines a saddle point; the zeta-prescription corresponds to running the evolution from this point, after reinstating path invariance. The equations for the special equipotential lines in the figure correspond to the one-loop result.

by supplementing γ_F with formally higher-order terms. If we let F be a generic TMD, then the evolution kernel R, implicitly defined as

$$F(x, \boldsymbol{b}, \mu_f, \zeta_f) = R(\boldsymbol{b}; \mu_f, \zeta_f; \mu_i, \zeta_i) F(x, \boldsymbol{b}, \mu_i, \zeta_i), \tag{C.17}$$

within the improved γ solution yields

$$R(\boldsymbol{b}; \mu_f, \zeta_f; \mu_i, \zeta_i) = \exp \left\{ \mathcal{D}(\mu_f, \boldsymbol{b}) \ln \left(\frac{\mu_f^2}{\zeta_f} \right) - \mathcal{D}(\mu_i, \boldsymbol{b}) \ln \left(\frac{\mu_i^2}{\zeta_i} \right) - \int_{\mu_i}^{\mu_f} \frac{d\mu}{\mu} \left[2\mathcal{D}(\mu, \boldsymbol{b}) + \gamma_V(\mu) \right] \right\}, \tag{C.18}$$

where γ_V is the noncusp anomalous dimension.

Path independence allows one to apply the ζ-*prescription*, the key point of the method. The idea is setting the initial rapidity scale $\zeta_i = \zeta_{\mu_i}$ as a function of μ_i such that the scale-dependence of the initial TMDs vanishes independent of μ_i. At one loop, this simply reads

$$\zeta_\mu = e^{-\frac{\gamma_V}{\Gamma_{\rm cusp}}} \mu^2, \tag{C.19}$$

and the corrections to higher loops are evaluated in [33].

The relation between ζ and μ draws a line in the $(\ln \zeta, \ln \mu^2)$ plane (figure 12). Since by requirement the TMDs are constant along it, this must be an equipotential line, which is well defined only if path-independence is restored. The remarkable fact with the ζ prescription is that, contrarily from standard evolution, the cancellation of large rapidity logarithms affecting the un-evolved TMDs is an internal mechanism. The rapidity evolution

is still responsible for cancelling the large logarithms in the hard function, but the scale uncertainty of the evolution is now entirely decoupled from the definition of the TMDs (and in particular, from the non-perturbative model that enters their definition).

The definition of *optimal TMDs* requires one more specification, which concerns the choice of initial scale μ_i (and consequently ζ_{μ_i}), and follows from TMD factorization. Considering TMD PDFs for definiteness, we have up to nonperturbative corrections

$$F_{a\leftarrow h}(x, \boldsymbol{b}, \mu, \zeta_\mu) = \sum_b \int_x^1 \frac{dy}{y} \, \mathcal{C}_{a\leftarrow b}(\tfrac{x}{y}, \boldsymbol{b}, \mu, \zeta_\mu, \mu_{\mathrm{OPE}}) f_{b\leftarrow h}(y, \mu_{\mathrm{OPE}}) \Big[1 + \mathcal{O}\big(b^2 \Lambda_{\mathrm{QCD}}^2\big)\Big] \,, \tag{C.20}$$

where $f_{b\leftarrow h}$ are the collinear PDFs, $\mathcal{C}_{a\leftarrow b}$ are transverse momentum matching coefficients known at two loop from ref. [31]. The matching is performed at the scale μ_{OPE}. The choice of μ_{OPE} is in general constrained by μ_i, as they need to lie on the same half-plane with respect to the saddle point. This undesired feature is eliminated by choosing $\mu_i = \mu_{\mathrm{saddle}}$.

C.4 Modeling of TMDPDF

At small transverse momenta non-perturbative effects inside a TMD become dominant. A non-perturbative model valid for optimal TMDs was recently extracted in ref. [45] by fitting combined data from Drell-Yan and Z-boson production. Since our groomed jet functions have the same rapidity evolution as the standard TMDs we will use the same model. First, for large values of b the initial scale, μ_{saddle} enters the non-perturbative region. We correct for this by adopting the definition

$$\mu_i = \frac{2e^{-\gamma_E}}{b} + 2\,\mathrm{GeV}\,, \tag{C.21}$$

which effectively imposes a higher cutoff on b. Second, the rapidity anomalous dimension is modified as follows,

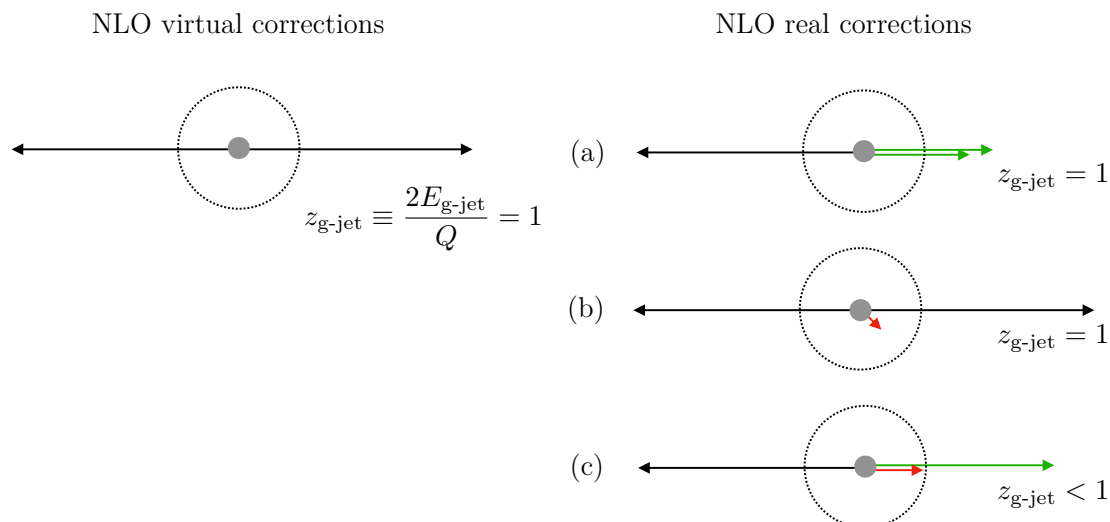$$\mathcal{D}(\mu, \boldsymbol{b}) = \mathcal{D}_{\mathrm{res}}(\mu, \boldsymbol{b}^*) + c_0 b\, b^* \,, \tag{C.22}$$

where c_0 is a constant, the resummed anomalous dimension can be found at three loop in refs. [33, 36], and the b-star prescription is

$$\boldsymbol{b}^* = \boldsymbol{b} \left(1 + \frac{b^2}{B_{\mathrm{NP}}^2}\right)^{-\frac{1}{2}} \,. \tag{C.23}$$

The constants c_0 and B_{NP} specify the nonpertubative model in the case of $e^+ e^- \to$ 2 jets. For SIDIS, additional input is required when building the TMD PDFs. Non-perturbative corrections to the factorization formula are modeled with a multiplicative, flavor-independent function f_{NP},

$$F_{a\leftarrow h}(x, \boldsymbol{b}, \mu, \zeta_\mu) = f_{\mathrm{NP}}(\boldsymbol{b}, x) \sum_b \int_x^1 \frac{dy}{y} \, \mathcal{C}_{a\leftarrow b}(\tfrac{x}{y}, \boldsymbol{b}, \mu, \zeta_\mu, \mu_{\mathrm{OPE}}) f_{b\leftarrow h}(y, \mu_{\mathrm{OPE}}) \,, \tag{C.24}$$

$$z_{\text{g-jet}} \equiv \frac{2E_{\text{g-jet}}}{Q} = 1$$

(a) $\quad z_{\text{g-jet}} = 1$

(b) $\quad z_{\text{g-jet}} = 1$

(c) $\quad z_{\text{g-jet}} < 1$

Figure 13. IR divergent configurations for soft-drop groomed jets at $\mathcal{O}(\alpha_s)$.

whose explicit expression reads

$$f_{\text{NP}}(\boldsymbol{b}, x) = \exp\left\{-\frac{\lambda_1(1-x) + \lambda_2 x + \lambda_3 x(1-x)}{\sqrt{1 + \lambda_4 x^{\lambda_5} b^2}} b^2\right\}, \tag{C.25}$$

generalizing the common choices of gaussian or exponential functions. The five parameters λ_i, together with c_0 and B_{NP}, are listed in table 4 of ref. [45] and were fitted within two different schemes: the first one treats them all as free parameters, while in the second one B_{NP} is fixed to 2.5 GeV^{-1}. The set of PDF used is NNPDF3.1 [54].

D IRC safety of the observable

It is known that the energy difference between groomed and ungroomed jet is an IRC unsafe quantity [15, 25]. For the lepton-antilepton annihilation process it is trivial to show even at the leading non vanishing order, $\mathcal{O}(\alpha_s)$. In the standard jet cross section the collinear and soft divergence from the additional real gluon cancel against the IR divergences form virtual contribution. This is possible because in both the collinear and soft limits ($p^0_{\text{gluon}} \to 0$ and $p^\mu_{\text{gluon}} \parallel p^\mu_{q/\bar{q}}$) the energy of the (ungroomed) jet, E_{jet}, equals half of the center of mass energy, Q, i.e. $z_{\text{jet}} \equiv 2E_{\text{jet}}/Q = 1$. In the case of groomed jets the phase space condition $p^\mu_{\text{gluon}} \parallel p^\mu_{q/\bar{q}}$ does not guarantee $z_{\text{g-jet}} = 1$ where $z_{\text{g-jet}}$ is the energy fraction fo the groomed jet, $z_{\text{g-jet}} \equiv 2E_{\text{g-jet}}/Q$. This is demonstrated in figure 13 where configuration (a) corresponds to collinear gluon emission that passes soft-drop ($p^\mu_{\text{gluon}} \parallel p^\mu_{q/\bar{q}}$ and $p^0_{\text{gluon}} > z_{\text{cut}}Q$), (b) soft gluon emission ($p^0_{\text{gluon}} \to 0$), (c) collinear gluon emission that fails soft-drop ($p^\mu_{\text{gluon}} \parallel p^\mu_{q/\bar{q}}$ and $p^0_{\text{gluon}} < z_{\text{cut}}Q$). While divergences from the phase space configurations (a) and (b) can cancel against the virtual divergences, the ones in configuration (c) cannot.

This problem is usually solved when a jet substructure measurement (e.g. jet thrust e) is included. In this case the configuration (c) will only contribute to the $e = 0$ bin and thus

does not constitute a problem of IRC safety, if we constrain the result for finite values of the jet thrust. In the observable we propose, the jet thrust measurement does not help since we require integrating over the range $e \in (0, e_{\text{cut}})$, see for example eq. (2.13). However, the transverse momentum $\boldsymbol{q}_T$ does since configuration (c) yields only $\boldsymbol{q}_T = 0$ and we are interested only in finite values of the transverse momentum. Therefore in our proposed observable the $\boldsymbol{q}_T$ measurement regulates the IRC divergences in a similar manner to the (differential) jet-shape measurements.

Furthermore is important to notice that the quantity $\boldsymbol{p}_{T \text{ g-jet}}/z_{\text{g-jet}}$ does not directly relate to groomed jet energy, but rather to the groomed jet direction, which is collinear safe to all orders in α_s,

$$\frac{\boldsymbol{p}_{T \text{ g-jet}}}{z_{\text{g-jet}}} = Q \sin(\theta_{\text{g-jet}}) \boldsymbol{n}_{T \text{ g-jet}} \tag{D.1}$$

where $\theta_{\text{g-jet}}$ is the angle between the groomed jet axis and the reference axis $\boldsymbol{n}_{T \text{ g-jet}}$ is the direction of the groomed jet with respect to the reference axis. Since the direction of the groomed jet is IR safe then the observable $\boldsymbol{q}_T$ is as well.

References

[1] J. Collins, *Foundations of perturbative QCD, Camb. Monogr. Part. Phys. Nucl. Phys. Cosmol.* **32** (2011) 1 [INSPIRE].

[2] M.G. Echevarria, A. Idilbi and I. Scimemi, *Factorization Theorem For Drell-Yan At Low q_T And Transverse Momentum Distributions On-The-Light-Cone, JHEP* **07** (2012) 002 [arXiv:1111.4996] [INSPIRE].

[3] M.G. Echevarria, A. Idilbi and I. Scimemi, *Unified treatment of the QCD evolution of all (un-)polarized transverse momentum dependent functions: Collins function as a study case, Phys. Rev.* **D 90** (2014) 014003 [arXiv:1402.0869] [INSPIRE].

[4] J.R. Gaunt, *Glauber Gluons and Multiple Parton Interactions, JHEP* **07** (2014) 110 [arXiv:1405.2080] [INSPIRE].

[5] A. Vladimirov, *Structure of rapidity divergences in multi-parton scattering soft factors, JHEP* **04** (2018) 045 [arXiv:1707.07606] [INSPIRE].

[6] D. Neill, I. Scimemi and W.J. Waalewijn, *Jet axes and universal transverse-momentum-dependent fragmentation, JHEP* **04** (2017) 020 [arXiv:1612.04817] [INSPIRE].

[7] D. Gutierrez-Reyes, I. Scimemi, W.J. Waalewijn and L. Zoppi, *Transverse momentum dependent distributions with jets, Phys. Rev. Lett.* **121** (2018) 162001 [arXiv:1807.07573] [INSPIRE].

[8] D. Gutierrez-Reyes, I. Scimemi, W.J. Waalewijn and L. Zoppi, *Transverse momentum dependent distributions in e^+e^- and semi-inclusive deep-inelastic scattering using jets,* arXiv:1904.04259 [INSPIRE].

[9] D. Bertolini, T. Chan and J. Thaler, *Jet Observables Without Jet Algorithms, JHEP* **04** (2014) 013 [arXiv:1310.7584] [INSPIRE].

[10] Y. Makris, D. Neill and V. Vaidya, *Probing Transverse-Momentum Dependent Evolution With Groomed Jets*, *JHEP* **07** (2018) 167 [arXiv:1712.07653] [INSPIRE].

[11] Y. Makris and V. Vaidya, *Transverse Momentum Spectra at Threshold for Groomed Heavy Quark Jets*, *JHEP* **10** (2018) 019 [arXiv:1807.09805] [INSPIRE].

[12] A.H. Hoang, S. Mantry, A. Pathak and I.W. Stewart, *Nonperturbative Corrections to Soft Drop Jet Mass*, arXiv:1906.11843 [INSPIRE].

[13] T. Sjöstrand, S. Mrenna and P.Z. Skands, *PYTHIA 6.4 Physics and Manual*, *JHEP* **05** (2006) 026 [hep-ph/0603175] [INSPIRE].

[14] T. Sjöstrand, S. Mrenna and P.Z. Skands, *A Brief Introduction to PYTHIA 8.1*, *Comput. Phys. Commun.* **178** (2008) 852 [arXiv:0710.3820] [INSPIRE].

[15] A.J. Larkoski, S. Marzani, G. Soyez and J. Thaler, *Soft Drop*, *JHEP* **05** (2014) 146 [arXiv:1402.2657] [INSPIRE].

[16] S.D. Ellis and D.E. Soper, *Successive combination jet algorithm for hadron collisions*, *Phys. Rev.* **D 48** (1993) 3160 [hep-ph/9305266] [INSPIRE].

[17] S. Catani, Y.L. Dokshitzer, M.H. Seymour and B.R. Webber, *Longitudinally invariant K_t clustering algorithms for hadron hadron collisions*, *Nucl. Phys.* **B 406** (1993) 187 [INSPIRE].

[18] Y.L. Dokshitzer, G.D. Leder, S. Moretti and B.R. Webber, *Better jet clustering algorithms*, *JHEP* **08** (1997) 001 [hep-ph/9707323] [INSPIRE].

[19] M. Wobisch and T. Wengler, *Hadronization corrections to jet cross-sections in deep inelastic scattering*, in *Monte Carlo generators for HERA physics. Proceedings, Workshop, Hamburg, Germany, 1998–1999*, pp. 270–279, (1998), hep-ph/9907280 [INSPIRE].

[20] M. Wobisch, *Measurement and QCD analysis of jet cross-sections in deep inelastic positron proton collisions at $\sqrt{s} = 300\,GeV$*, Ph.D. Thesis, Aachen, Tech. Hochsch., (2000).

[21] M. Cacciari, G.P. Salam and G. Soyez, *The anti-k_t jet clustering algorithm*, *JHEP* **04** (2008) 063 [arXiv:0802.1189] [INSPIRE].

[22] G. Salam, E_t^∞ *Scheme*, unpublished.

[23] A.J. Larkoski, D. Neill and J. Thaler, *Jet Shapes with the Broadening Axis*, *JHEP* **04** (2014) 017 [arXiv:1401.2158] [INSPIRE].

[24] S. Marzani, L. Schunk and G. Soyez, *A study of jet mass distributions with grooming*, *JHEP* **07** (2017) 132 [arXiv:1704.02210] [INSPIRE].

[25] A.J. Larkoski, S. Marzani and J. Thaler, *Sudakov Safety in Perturbative QCD*, *Phys. Rev.* **D 91** (2015) 111501 [arXiv:1502.01719] [INSPIRE].

[26] J.-Y. Chiu, A. Jain, D. Neill and I.Z. Rothstein, *A Formalism for the Systematic Treatment of Rapidity Logarithms in Quantum Field Theory*, *JHEP* **05** (2012) 084 [arXiv:1202.0814] [INSPIRE].

[27] M.G. Echevarria, I. Scimemi and A. Vladimirov, *Universal transverse momentum dependent soft function at NNLO*, *Phys. Rev.* **D 93** (2016) 054004 [arXiv:1511.05590] [INSPIRE].

[28] Y. Li and H.X. Zhu, *Bootstrapping Rapidity Anomalous Dimensions for Transverse-Momentum Resummation*, *Phys. Rev. Lett.* **118** (2017) 022004 [arXiv:1604.01404] [INSPIRE].

[29] A.A. Vladimirov, *Correspondence between Soft and Rapidity Anomalous Dimensions*, *Phys. Rev. Lett.* **118** (2017) 062001 [arXiv:1610.05791] [INSPIRE].

[30] I. Scimemi and A. Vladimirov, *Power corrections and renormalons in Transverse Momentum Distributions*, *JHEP* **03** (2017) 002 [`arXiv:1609.06047`] [INSPIRE].

[31] M.G. Echevarria, I. Scimemi and A. Vladimirov, *Unpolarized Transverse Momentum Dependent Parton Distribution and Fragmentation Functions at next-to-next-to-leading order*, *JHEP* **09** (2016) 004 [`arXiv:1604.07869`] [INSPIRE].

[32] M. Cacciari, G.P. Salam and G. Soyez, *FastJet User Manual*, *Eur. Phys. J.* **C 72** (2012) 1896 [`arXiv:1111.6097`] [INSPIRE].

[33] I. Scimemi and A. Vladimirov, *Systematic analysis of double-scale evolution*, *JHEP* **08** (2018) 003 [`arXiv:1803.11089`] [INSPIRE].

[34] T. Gehrmann, T. Luebbert and L.L. Yang, *Calculation of the transverse parton distribution functions at next-to-next-to-leading order*, *JHEP* **06** (2014) 155 [`arXiv:1403.6451`] [INSPIRE].

[35] U. D'Alesio, M.G. Echevarria, S. Melis and I. Scimemi, *Non-perturbative QCD effects in q_T spectra of Drell-Yan and Z-boson production*, *JHEP* **11** (2014) 098 [`arXiv:1407.3311`] [INSPIRE].

[36] M.G. Echevarria, A. Idilbi, A. Schäfer and I. Scimemi, *Model-Independent Evolution of Transverse Momentum Dependent Distribution Functions (TMDs) at NNLL*, *Eur. Phys. J.* **C 73** (2013) 2636 [`arXiv:1208.1281`] [INSPIRE].

[37] J.-y. Chiu, A. Jain, D. Neill and I.Z. Rothstein, *The Rapidity Renormalization Group*, *Phys. Rev. Lett.* **108** (2012) 151601 [`arXiv:1104.0881`] [INSPIRE].

[38] S. Moch, J.A.M. Vermaseren and A. Vogt, *The three loop splitting functions in QCD: The nonsinglet case*, *Nucl. Phys.* **B 688** (2004) 101 [`hep-ph/0403192`] [INSPIRE].

[39] S. Moch, J.A.M. Vermaseren and A. Vogt, *Three-loop results for quark and gluon form-factors*, *Phys. Lett.* **B 625** (2005) 245 [`hep-ph/0508055`] [INSPIRE].

[40] P.A. Baikov, K.G. Chetyrkin, A.V. Smirnov, V.A. Smirnov and M. Steinhauser, *Quark and gluon form factors to three loops*, *Phys. Rev. Lett.* **102** (2009) 212002 [`arXiv:0902.3519`] [INSPIRE].

[41] A. Vogt, F. Herzog, S. Moch, B. Ruijl, T. Ueda and J.A.M. Vermaseren, *Anomalous dimensions and splitting functions beyond the next-to-next-to-leading order*, `PoS(LL2018)050` (2018) [`arXiv:1808.08981`] [INSPIRE].

[42] C.W. Bauer, F.J. Tackmann, J.R. Walsh and S. Zuberi, *Factorization and Resummation for Dijet Invariant Mass Spectra*, *Phys. Rev.* **D 85** (2012) 074006 [`arXiv:1106.6047`] [INSPIRE].

[43] C. Frye, A.J. Larkoski, M.D. Schwartz and K. Yan, *Factorization for groomed jet substructure beyond the next-to-leading logarithm*, *JHEP* **07** (2016) 064 [`arXiv:1603.09338`] [INSPIRE].

[44] D. Kang, C. Lee and I.W. Stewart, *Using 1-Jettiness to Measure 2 Jets in DIS 3 Ways*, *Phys. Rev.* **D 88** (2013) 054004 [`arXiv:1303.6952`] [INSPIRE].

[45] V. Bertone, I. Scimemi and A. Vladimirov, *Extraction of unpolarized quark transverse momentum dependent parton distributions from Drell-Yan/Z-boson production*, *JHEP* **06** (2019) 028 [`arXiv:1902.08474`] [INSPIRE].

[46] M. Beneke and V.M. Braun, *Power corrections and renormalons in Drell-Yan production*, *Nucl. Phys.* **B 454** (1995) 253 [`hep-ph/9506452`] [INSPIRE].

[47] G.P. Korchemsky and G.F. Sterman, *Nonperturbative corrections in resummed cross-sections*, *Nucl. Phys.* **B 437** (1995) 415 [`hep-ph/9411211`] [INSPIRE].

[48] G.P. Korchemsky, G. Oderda and G.F. Sterman, *Power corrections and nonlocal operators*, *AIP Conf. Proc.* **407** (1997) 988 [`hep-ph/9708346`] [ɪɴSPIRE].

[49] M. Beneke, V.M. Braun and L. Magnea, *Phenomenology of power corrections in fragmentation processes in e^+e^- annihilation*, *Nucl. Phys.* **B 497** (1997) 297 [`hep-ph/9701309`] [ɪɴSPIRE].

[50] T. Becher and G. Bell, *Enhanced nonperturbative effects through the collinear anomaly*, *Phys. Rev. Lett.* **112** (2014) 182002 [`arXiv:1312.5327`] [ɪɴSPIRE].

[51] `artemide` web-page, https://teorica.fis.ucm.es/artemide/.

[52] `artemide` repository, https://github.com/vladimirovalexey/artemide-public.

[53] I. Scimemi and A. Vladimirov, *Analysis of vector boson production within TMD factorization*, *Eur. Phys. J.* **C 78** (2018) 89 [`arXiv:1706.01473`] [ɪɴSPIRE].

[54] NNPDF collaboration, *Parton distributions from high-precision collider data*, *Eur. Phys. J.* **C 77** (2017) 663 [`arXiv:1706.00428`] [ɪɴSPIRE].